AIMS Mathematics, 10(10): 22817–22849.
DOI: 10.3934/math.20251014
Received: 04 August 2025
Revised: 07 September 2025
Accepted: 18 September 2025
Published: 09 October 2025

https://www.aimspress.com/journal/Math

Research article

Numerical simulation of a fractional glucose-insulin model via successive approximation and ABM schemes

Muflih Alhazmi[1], **Safa M. Mirgani**[2], **A. F. Aljohani**[3] **and Sayed Saber**[4,5,*]

[1] Mathematics Department, Faculty of Science, Northern Border University, Arar, Saudi Arabia

[2] Imam Mohammad Ibn Saud Islamic University (IMSIU), College of Science, Department of Mathematics and Statistics, Riyadh, Saudi Arabia

[3] Department of Mathematics, Faculty of Science, University of Tabuk, Tabuk, Saudi Arabia

[4] Department of Mathematics, Faculty of Science, Al-Baha University, Al-Baha, Saudi Arabia

[5] Department of Mathematics and Computer Science, Faculty of Science, Beni-Suef University, Beni-Suef, Egypt

* **Correspondence:** Email: Sayed011258@science.bsu.edu.eg; Tel: +9660597625063.

Abstract: We developed a fractional-order glucose–insulin regulatory model in the Caputo sense to encode memory effects in metabolic dynamics. The three-equation nonlinear system employed component-wise fractional orders to represent heterogeneous memory depths across plasma glucose, insulin action, and secretion. We established well-posedness (existence, uniqueness), positivity, and boundedness, and assess local stability; oscillatory regimes were further examined via discrete-time Hopf conditions for the discretized dynamics. For computation, we implement the successive approximation method (SAM) and a fractional Adams–Bashforth–Moulton (ABM) predictor–corrector scheme. In head-to-head tests, ABM achieved lower residuals, better stability, and higher efficiency than SAM, with validation against frequently sampled intravenous glucose tolerance test (FSIGT) data and a global sensitivity analysis highlighting insulin responsiveness and glucose-threshold parameters as most influential. Residual analysis indicated that increasing the fractional order(s) toward the integer case reduced numerical error—for example, the representative state error $|\Delta u|$ decreased from 129.6 at $\nu = 0.5$ to 34.1 at $\nu = 0.9$. These results supported the clinical relevance of fractional-order modeling for improved diabetes management, parameter tuning, and control strategy design.

Keywords: fractional derivatives, nonlinear equations, simulation, numerical results, iterative method, zoonotic disease
Mathematics Subject Classification: 34A08, 34L99, 92D30

1. Introduction

Mathematical modeling serves as a vital tool for deciphering the complex dynamics between glucose and insulin in the human body, a relationship that is paramount in understanding and managing diabetes mellitus [1–3]. Among the most influential frameworks is the minimal model, introduced by Bergman et al., which provides a parsimonious yet effective structure for interpreting data from intravenous glucose tolerance tests (IVGTT) [4]. This model successfully captures essential physiological mechanisms, including insulin-mediated glucose uptake and pancreatic insulin secretion.

Despite their widespread use and success, classical integer-order differential equation models possess a significant limitation: they often fail to capture the hereditary and memory-dependent behaviors intrinsic to metabolic systems [5–7]. These models typically assume Markovian behavior, where the future state depends only on the present, thereby neglecting the profound influence of past system states on current metabolic regulation [8]. This shortcoming has catalyzed a growing interest in fractional-order differential equations (FDEs), particularly those utilizing Caputo derivatives, which offer a natural and powerful mathematical framework for modeling systems with memory and long-range dependencies [9–11]. Recent advancements in fractional calculus have further enabled the incorporation of these memory effects through non-integer-order derivatives, such as those defined in the Caputo and Caputo–Fabrizio senses [12–15].

The application of FDEs is exceptionally well-suited to biological systems like glucose-insulin regulation, where the current physiological state is influenced not only by immediate conditions but also by a history of past states [16]. In this context, fractional-order models have demonstrated superior accuracy in simulating critical features such as time-delayed insulin responses, saturation in glucose uptake, and nonlinear secretion thresholds [17–19]. Consequently, these models have shown a marked improvement in fitting real patient data and IVGTT results compared to their integer-order counterparts [20, 21].

This paper introduces a novel fractional-order glucose-insulin regulatory model based on Caputo derivatives to describe the dynamics of plasma glucose concentration, insulin action, and insulin secretion. A key innovation of our model is the assignment of distinct fractional orders ν_1, ν_2, ν_3 to each state variable, allowing it to capture the varying memory depths inherent in different metabolic pathways.

To solve this model effectively, we implement and compare two advanced numerical schemes: the successive approximation method (SAM) [22] and the fractional Adams–Bashforth–Moulton (ABM) predictor-corrector method [10]. While SAM provides valuable analytical series approximations that offer insight into the solution structure, the ABM method delivers stable and accurate time integration for the system's nonlocal dynamics. Moving beyond simulation, we conduct a comprehensive sensitivity analysis to identify which parameters exert the strongest influence on system behavior. This analysis is crucial for pinpointing potential targets for therapeutic intervention and for parameter tuning in clinical applications [22, 23]. To ensure physiological relevance, our approach is validated against real experimental data from frequently sampled intravenous glucose tolerance test (FSIGT) studies [9]. Recent advances show that fractal-fractional operators can effectively capture infection dynamics in biological systems such as pneumococcal pneumonia [24]. The analytical foundation of our model is rigorously established through proofs of fundamental properties, including the existence, uniqueness, nonnegativity, and boundedness of solutions. We further examine local stability using

eigenvalue analysis and apply discrete-time Hopf bifurcation theory to assess the potential emergence of oscillatory behavior near equilibrium points [25, 26]. In summary, the proposed framework significantly enhances the understanding of glucose-insulin regulatory dynamics. Its implications extend to the design of robust control strategies, the refinement of artificial pancreas algorithms, and the development of personalized treatment protocols, thereby bridging a critical gap between mathematical theory and clinical practice [27].

Mathematical models are indispensable tools for exploring complex physiological processes such as glucose-insulin regulation. They enable quantitative predictions and provide a foundation for designing effective therapeutic interventions [28]. The minimal model remains one of the most widely used frameworks for interpreting IVGTT data via a compact system of differential equations [29]. fractional models have proven highly successful in capturing long-term dependencies across various physiological and epidemiological contexts [30]. Within glucose-insulin regulation, recent studies have introduced fractional frameworks to more accurately simulate insulin response delays, glucose uptake saturation, and β-cell feedback mechanisms [31].

In this study, we formulate a fractional-order glucose-insulin model utilizing Caputo derivatives of distinct orders for plasma glucose, insulin effectiveness, and insulin secretion. The system incorporates essential nonlinearities through a positive-part operator $[\cdot]^+$ to realistically model insulin secretion thresholds. To solve the model numerically, we employ two efficient fractional schemes: the SAM [22] and the ABM methods, adapted for fractional differential systems [10, 32]. SAM yields explicit series approximations, while ABM provides high-order accuracy in time discretization. Our theoretical analysis encompasses proofs of nonnegativity, boundedness, existence, and uniqueness of solutions [33, 34]. We investigate local stability through Jacobian analysis and extend our examination to bifurcation behavior using discrete-time Hopf bifurcation theory [25]. A thorough sensitivity analysis is conducted to identify the parameters with the greatest influence on system outputs [23]. This work builds upon and extends prior research on fractional glucose-insulin models [35–37], chaotic systems with memory [38–40], and disease modeling with fractional and fractal-fractional operators [41]. Our approach synergizes mathematical rigor, numerical efficiency, and physiological realism, offering a robust framework for future applications in diabetes control, optimal therapy design, and fractional feedback stabilization [42–46].

The primary aim of this study is to develop and analyze a fractional-order glucose–insulin regulatory model that effectively captures the memory-dependent behavior of glucose metabolism using Caputo derivatives. Our specific objectives are to:

- Formulate a physiologically consistent fractional-order model describing the dynamics of plasma glucose, insulin action, and insulin secretion.
- Implement and compare two numerical solution techniques—the SAM and ABM methods.
- Validate the fractional model using experimental FSIGT data.
- Perform residual and sensitivity analyses to evaluate numerical accuracy and identify the most influential physiological parameters.
- Explore the biological relevance of fractional-order dynamics for designing improved control strategies in diabetes management.

The motivation for this research stems from the inherent limitations of integer-order models, which inadequately capture the hereditary and memory effects that are fundamental to metabolic regulation.

Glucose-insulin dynamics are profoundly influenced by past system states, including delayed insulin responses, cumulative glucose exposure, and long-term feedback mechanisms. fractional-order derivatives, particularly in the Caputo sense, provide a natural mathematical framework for incorporating such memory-dependent processes. By adopting a fractional-order formulation, we aim to achieve a more physiologically realistic representation of glucose-insulin interactions, enhance the fidelity of numerical simulations, and generate novel insights for developing therapeutic strategies.

The novelty of our work lies in the comprehensive integration of mathematical theory, numerical simulation, and physiological validation within a unified fractional-order modeling framework. Specifically, we: (i) formulate a fractional glucose-insulin system with distinct Caputo derivatives to represent heterogeneous memory depth across metabolic compartments; (ii) establish fundamental analytical properties, including nonnegativity, boundedness, existence, uniqueness, stability, and bifurcation behavior; (iii) implement and compare two powerful numerical schemes—SAM and the fractional ABM predictor-corrector method—to rigorously assess accuracy and efficiency; (iv) validate the model against experimental FSIGT data to ensure physiological relevance; and (v) conduct sensitivity analysis to identify the most influential parameters for therapeutic intervention. By combining theoretical rigor, robust numerical methods, and validation with experimental data, this work contributes a novel and physiologically consistent framework for the fractional-order modeling of glucose-insulin dynamics. This framework holds significant potential for applications in artificial pancreas design, personalized diabetes therapy, and the development of advanced control strategies.

Establishing a strong analytical foundation is as crucial as numerical simulation for the proposed model. Proofs of existence and uniqueness guarantee that the fractional glucose-insulin system is mathematically well-posed, ensuring that numerical solutions are meaningful and correspond to a biologically consistent process. Demonstrating nonnegativity and boundedness confirms that the model adheres to physiological constraints, such as the necessity for positive concentrations of glucose and insulin. Local stability analysis provides critical insight into whether equilibrium states (e.g., fasting glucose and basal insulin levels) remain stable under small perturbations, which is fundamental for distinguishing normal homeostasis from pathological regulation. Furthermore, the application of Hopf bifurcation theory extends previous fractional models by characterizing the conditions under which oscillatory or unstable glucose-insulin dynamics may emerge, offering a theoretical explanation for clinically observed phenomena like glycemic variability. This rigorous analytical framework advances the field beyond studies that focus primarily on numerical fitting or qualitative dynamics, thereby strengthening both the reliability and interpretability of our model.

The guarantees of positivity and boundedness ensure physiologically admissible states during parameter estimation and data assimilation. Insights from local stability and Hopf bifurcation analysis inform controller design and help interpret complex oscillatory behaviors. Existence and uniqueness results on finite time horizons provide the well-posedness necessary for inverse problems and parameter identifiability studies. Our contribution tailors these guarantees specifically to a *component-wise* fractional system featuring a threshold nonlinearity, and presents them in a form that is directly usable by the SAM and ABM discretizations—addressing regularity away from $t = 0$, residual-based accuracy, and empirical convergence.

The remainder of the paper is organized as follows. In Section 2, the fractional-order glucose–insulin regulatory model is formulated and the biological interpretation of its functions is provided. Section 3 establishes the theoretical properties of the system, including nonnegativity, boundedness,

existence, and uniqueness of solutions. Section 4 presents the local stability analysis of the equilibrium point, while Section 5 explores the Hopf bifurcation conditions. Section 6 is devoted to residual and sensitivity analyses, highlighting the most influential physiological parameters. Section 7 describes the applied numerical techniques, namely the SAM and ABM schemes, followed by simulation results. Section 8 provides a detailed discussion of the findings and their clinical implications. Finally, Section 9 concludes the study by summarizing the main contributions and outlining directions for future research.

2. Model functions and their biological interpretations

In this system, u (mg/dL) and w (mU/L) denote plasma glucose and insulin concentrations at time t (min), respectively. The auxiliary state v (1/min) models the insulin–dependent tissue glucose uptake rate. The constants u_b and w_b are the basal (fasting) glucose and insulin levels. Parameter p_1 quantifies insulin–independent glucose clearance; p_2, p_3, p_4, and p_6 govern insulin action and secretion; and p_5 is the glucose threshold that triggers insulin release.

The classical (integer–order) *minimal model* with insulin kinetics [47] is

$$\begin{aligned} \frac{du}{dt} &= -(p_1 + v)\,u + p_1\,u_b, \\ \frac{dv}{dt} &= -p_2\,v + p_3\,(w - w_b), \\ \frac{dw}{dt} &= p_4\,[u - p_5]^+ - p_6\,(w - w_b), \end{aligned} \tag{2.1}$$

with the nonlinear threshold

$$[u - p_5]^+ \;=\; \begin{cases} u - p_5, & u > p_5, \\ 0, & u \le p_5, \end{cases} \qquad u(0) = b_0, \quad v(0) = 0, \quad w(0) = w_b.$$

To incorporate physiological memory, we use the Caputo derivative and the Riemann–Liouville fractional integral, with lower limit 0. For $q > 0$ and $f \in L^1_{\mathrm{loc}}(0, T)$,

$$(I^{\nu}_{0,t} f)(t) \;=\; \frac{1}{\Gamma(\nu)} \int_0^t (t - \tau)^{\nu - 1} f(\tau)\, d\tau,$$

and, for $\nu \in (n - 1, n)$ with $n \in \mathbb{N}$ and $f \in C^n[0, T]$,

$${}^{C}\mathscr{D}^{\nu}_{0,t} f(t) \;=\; (I^{n-\nu}_{0,t} f^{(n)})(t) \;=\; \frac{1}{\Gamma(n - \nu)} \int_0^t (t - \tau)^{n-\nu-1}\, f^{(n)}(\tau)\, d\tau.$$

Let $\boldsymbol{\nu} = (\nu_1, \nu_2, \nu_3) \in (0, 1]^3$ assign a Caputo order to each state:

$$\begin{aligned} {}^{C}\mathscr{D}^{\nu_1}_{0,t} u(t) &= -(p_1 + v(t))\,u(t) + p_1\,u_b, \\ {}^{C}\mathscr{D}^{\nu_2}_{0,t} v(t) &= -p_2\,v(t) + p_3\,(w(t) - w_b), \\ {}^{C}\mathscr{D}^{\nu_3}_{0,t} w(t) &= p_4\,[u(t) - p_5]^+ - p_6\,(w(t) - w_b), \end{aligned} \tag{2.2}$$

with the same initial conditions $u(0) = b_0$, $v(0) = 0$, $w(0) = w_b$. The fractional formulation captures delayed feedback and history–dependence across compartments via the orders ν_i, while preserving physiologically admissible (Caputo) initial conditions.

Remark 2.1. *For well–posedness on* $[0, T]$*, we assume* $f(t, \mathbf{y})$ *in* (2.2) *is continuous in* t*, locally Lipschitz in* $\mathbf{y} = (u, v, w)$*, and of at most linear growth; these minimal conditions replace earlier vague phrases such as "sufficiently smooth". Additional* C^1 *regularity in* $\mathbf{y}$ *is invoked only for Jacobian–based stability analysis.*

2.1. Physiological and kinetic justification for the fractional formulation

The transition from the classical system (2.1) to the fractional system (2.2) is not merely formal; it follows from a hereditary (distributed–delay) representation of glucose–insulin physiology. Many processes in this axis—including insulin receptor binding and internalization, intracellular signaling cascades (e.g., glucose transporter type 4 (GLUT4) translocation), hepatic/renal clearance, and tissue uptake—exhibit broad, heterogeneous timescales. A standard way to encode such heterogeneity is to replace the instantaneous rate in each balance law by a convolution with a memory kernel $K(t)$:

$$\frac{d}{dt}x(t) = F(x(t)) + \int_0^t K(t-s)\, G(x(s))\, ds,$$

where x denotes u, v, w and F, G collect the local terms in (2.1).* When K is completely monotone with a power-law tail,

$$K_{1-\nu}(t) = \frac{t^{-\nu}}{\Gamma(1-\nu)}, \qquad 0 < \nu < 1,$$

the hereditary operator becomes the Riemann–Liouville fractional integral $I^{1-\nu}$ and, using the identity ${}^{C}\mathscr{D}^{\nu}_{0,t}x = I^{1-\nu}\frac{d}{dt}x$ (Caputo derivative), the hereditary balance reduces to a fractional differential law

$${}^{C}\mathscr{D}^{\nu}_{0,t}x(t) = F(x(t)) + G(x(t)),$$

which is precisely the structure used in (2.2). This yields a mechanistic interpretation of the fractional orders ν_1, ν_2, ν_3: they quantify the effective memory depth of, respectively, plasma glucose, insulin action, and insulin secretion compartments, reflecting different degrees of physiological heterogeneity and distributed delays.

Concretely, starting from (2.1), we apply $I^{1-\nu_i}$ to each equation (with possibly distinct orders $\nu_i \in (0, 1)$ dictated by the underlying kernel of each pathway) and use ${}^{C}\mathscr{D}^{\nu_i}_{0,t}x = I^{1-\nu_i}\frac{d}{dt}x$ to obtain system (2.2). This derivation shows that the fractional model is the continuum-limit reduction of a physiologically grounded distributed-delay/compartmental description, not an ad hoc replacement. It also explains why fractional orders improve empirical fit and robustness: power-law memory compactly approximates a wide spectrum of hidden time constants, a feature supported by our validation against FSIGT data and the stability/sensitivity analyses presented later in the paper.

3. Nonnegativity, boundedness, existence, and uniqueness

Theorem 3.1. *If* $p_1, p_2, p_3, p_4, p_6 > 0$*, and* $\mathrm{u}_b, \mathrm{w}_b, p_5 \geq 0$*, then the solution* $(\mathrm{u}(t), \mathrm{v}(t), \mathrm{w}(t))$ *to system (2.2) with nonnegative initial conditions remains nonnegative for all* $t \geq 0$*.*

*See, e.g., hereditary/viscoelastic analogues in which macroscopic dynamics arise from parallel sums of linear compartments with a spectrum of time constants; in the continuum (heavy-tailed) limit, K becomes scale-free.

Proof. Assume by contradiction that one of the variables becomes negative for the first time at $t_0 > 0$.

For $\mathrm{u}(t)$, suppose $\mathrm{u}(t_0) = 0$. Then,

$$ {}^{C}\mathscr{D}_{0,t}^{\nu_1}\,\mathrm{u}(t_0) = -[p_1 + \mathrm{v}(t_0)] \cdot 0 + p_1\,\mathrm{u}_b = p_1\,\mathrm{u}_b \geq 0. $$

This implies that $\mathrm{u}(t)$ cannot decrease below zero.

For $\mathrm{v}(t)$, if $\mathrm{v}(t_0) = 0$, then

$$ {}^{C}\mathscr{D}_{0,t}^{\nu_2}\,\mathrm{v}(t_0) = -p_2 \cdot 0 + p_3[\mathrm{w}(t_0) - \mathrm{w}_b]. $$

If $\mathrm{w}(t_0) \geq \mathrm{w}_b$, this derivative is nonnegative.

For $\mathrm{w}(t)$, if $\mathrm{w}(t_0) = 0$, then

$$ {}^{C}\mathscr{D}_{0,t}^{\nu_3}\,\mathrm{w}(t_0) = p_4[\mathrm{u}(t_0) - p_5]^{+}t_0 + p_6\,\mathrm{w}_b \geq 0. $$

In all cases, the Caputo derivative at the boundary is nonnegative, implying that the solution cannot cross into the negative domain. Hence, the solutions remain nonnegative for all $t \geq 0$. □

We adopt:

(A1) Orders: $0 < \nu_i < 1$ for $i = 1, 2, 3$ and set $\nu := \max\{\nu_1, \nu_2, \nu_3\}$ and $\nu_* := \min\{\nu_1, \nu_2, \nu_3\}$.
(A2) Parameters: $p_1, p_2, p_3, p_4, p_6 > 0$ and $u_b, w_b, p_5 \geq 0$.
(A3) (Single-regime regularity) There exists $\delta > 0$ such that either $u(t) \geq p_5 + \delta$ on $[0, T]$ or $u(t) \leq p_5 - \delta$ on $[0, T]$.

Assumption (A3) ensures $[u - p_5]_+$ is C^1 *along the trajectory*. If the trajectory crosses $u = p_5$, all results hold piecewise on subintervals separated by the (finite) switching times; a C^1-mollified threshold can also be used (Remark 3.3).

Lemma 3.1 (fractional Grönwall)**.** *Let $0 < \beta \leq 1$, $A, B \geq 0$, and let $y \in C([0, T]; \mathbb{R}_{\geq 0})$ satisfy*

$$ y(t) \;\leq\; A \;+\; \frac{B}{\Gamma(\beta)} \int_0^t (t - s)^{\beta - 1}\, y(s)\, ds, \qquad t \in [0, T]. $$

Then $y(t) \leq A\, E_\beta\big(B\, t^\beta\big) \leq A\, E_\beta\big(B\, T^\beta\big)$, where $E_\beta(z) = \sum_{k=0}^{\infty} \frac{z^k}{\Gamma(\beta k + 1)}$ is the Mittag–Leffler function.

Proof. Let $\mathcal{V}z(t) := \frac{B}{\Gamma(\beta)} \int_0^t (t - s)^{\beta - 1} z(s)\, ds$. Define $y_0 \equiv A$ and $y_{n+1} := A + \mathcal{V}y_n$. Positivity of the kernel yields $0 \leq y_0 \leq y_1 \leq \cdots$ and $y \leq y_n$ for all n. By induction, $y_n(t) = A \sum_{k=0}^{n} \frac{(Bt^\beta)^k}{\Gamma(\beta k + 1)}$. Letting $n \to \infty$ gives the claim. □

Theorem 3.2 (C^1-nonnegativity and boundedness)**.** *Assume* (A1)–(A3) *and* $(u_0, v_0, w_0) \in \mathbb{R}^3_{\geq 0}$. *Let* $(u, v, w) \in C^1([0, T]; \mathbb{R}^3)$ *solve* (2.2) *in the Caputo sense. Then:*

(1) Nonnegativity. *$u(t), v(t), w(t) \geq 0$ for all $t \in [0, T]$.*
(2) Uniform boundedness. *There exists $B_T > 0$ (depending on the data and parameters) such that*

$$ 0 \;\leq\; u(t) + v(t) + w(t) \;\leq\; B_T, \qquad \forall\, t \in [0, T]. $$

Proof. Nonnegativity. As in the initial theorem, the righthand sides of (2.2) are nonnegative on the boundary of $\mathbb{R}^3_{\geq 0}$; with Caputo derivatives for C^1 functions, the standard barrier argument ensures nonnegativity for all $t \geq 0$.

Boundedness. Using the Caputo integral form (for $x \in \{u, v, w\}$),

$$x(t) = x_0 + \frac{1}{\Gamma(\nu_x)} \int_0^t (t-s)^{\nu_x - 1} f_x(u(s), v(s), w(s), s)\, ds,$$

and discarding nonpositive contributions, we obtain for $t \in [0, T]$:

$$\begin{aligned} u(t) &\leq u_0 + \frac{p_1 u_b}{\Gamma(\nu_1 + 1)}\, t^{\nu_1}, \\ v(t) &\leq v_0 + \frac{p_3}{\Gamma(\nu_2)} \int_0^t (t-s)^{\nu_2 - 1} w(s)\, ds, \\ w(t) &\leq w_0 + \frac{p_6 w_b}{\Gamma(\nu_3 + 1)}\, t^{\nu_3} + \frac{p_4}{\Gamma(\nu_3)} \int_0^t (t-s)^{\nu_3 - 1}\, s\, u(s)\, ds. \end{aligned}$$

Let $N(t) := u(t) + v(t) + w(t)$. Since $u(t), w(t) \geq 0$, we have $u(s), w(s) \leq N(s)$ for $s \in [0, t]$. Let $\nu_* = \min\{\nu_1, \nu_2, \nu_3\}$. Noting that $(t-s)^{\nu_i - 1} \leq (t-s)^{\nu_* - 1}$ for $i = 2, 3$ and $s \leq T$, we combine the inequalities:

$$\begin{aligned} N(t) \leq u_0 + v_0 + w_0 + \frac{p_1 u_b}{\Gamma(\nu_1 + 1)} T^{\nu_1} + \frac{p_6 w_b}{\Gamma(\nu_3 + 1)} T^{\nu_3} \\ + \frac{p_3}{\Gamma(\nu_2)} \int_0^t (t-s)^{\nu_* - 1} N(s)\, ds + \frac{p_4 T}{\Gamma(\nu_3)} \int_0^t (t-s)^{\nu_* - 1} N(s)\, ds. \end{aligned}$$

Define the constants:

$$A_T := N(0) + \frac{p_1 u_b}{\Gamma(\nu_1 + 1)} T^{\nu_1} + \frac{p_6 w_b}{\Gamma(\nu_3 + 1)} T^{\nu_3}, \quad B := \frac{p_3}{\Gamma(\nu_2)} + \frac{p_4 T}{\Gamma(\nu_3)}.$$

This yields the Volterra inequality:

$$N(t) \leq A_T + B \int_0^t (t-s)^{\nu_* - 1} N(s)\, ds.$$

To apply Lemma 3.1, we write the kernel in the normalized form:

$$N(t) \leq A_T + \frac{B\,\Gamma(\nu_*)}{\Gamma(\nu_*)} \int_0^t (t-s)^{\nu_* - 1} N(s)\, ds = A_T + \frac{B\,\Gamma(\nu_*)}{\Gamma(\nu_*)} \int_0^t (t-s)^{\nu_* - 1} N(s)\, ds.$$

Lemma 3.1 (with $\beta = \nu_*$ and constant $\widetilde{B} = B\,\Gamma(\nu_*)$) therefore implies:

$$N(t) \leq A_T\, E_{\nu_*}(B\,\Gamma(\nu_*)\, t^{\nu_*}) \leq A_T\, E_{\nu_*}(B\,\Gamma(\nu_*)\, T^{\nu_*}).$$

The claimed uniform bound follows by setting $B_T := A_T\, E_{\nu_*}(B\,\Gamma(\nu_*)\, T^{\nu_*})$. □

Remark 3.1. *Earlier we informally bounded $D_t^{\nu} N(t)$ by $C_1 + C_2 t$ and appealed to a "generalized Grönwall" inequality. Here we avoid that shortcut entirely: we work in the integral (Volterra) form, derive an explicit Volterra inequality with a positive, L^1 weakly singular kernel, and verify all hypotheses of the fractional Grönwall lemma before applying it. This delivers a rigorous, textbook application and a closed bound via the Mittag–Leffler function E_{ν_*}.*

Theorem 3.3 (C^1 local existence and uniqueness)**.** *Assume* (A1)–(A3). *Then there exists a unique solution* $(u, v, w) \in C^1([0, T]; \mathbb{R}^3_{\geq 0})$ *to the system* (2.2).

Proof. The proof proceeds by a standard contraction mapping argument on a short time interval, followed by continuation.

(1) Local existence and uniqueness. Let $\nu = \max\{\nu_1, \nu_2, \nu_3\}$. Rewrite the system in its Volterra form $\mathbf{x} = \mathbf{x}_0 + \mathcal{T}\mathbf{x}$, where $\mathbf{x} = (u, v, w)^\top$, $\mathbf{x}_0 = (u_0, v_0, w_0)^\top$, and the operator $\mathcal{T}$ is defined by

$$(\mathcal{T}\mathbf{x})(t) = \begin{pmatrix} \frac{1}{\Gamma(\nu_1)} \int_0^t (t-s)^{\nu_1 - 1} F_1(\mathbf{x}(s), s)\, ds \\ \frac{1}{\Gamma(\nu_2)} \int_0^t (t-s)^{\nu_2 - 1} F_2(\mathbf{x}(s), s)\, ds \\ \frac{1}{\Gamma(\nu_3)} \int_0^t (t-s)^{\nu_3 - 1} F_3(\mathbf{x}(s), s)\, ds \end{pmatrix},$$

with F_1, F_2, F_3 being the righthand sides of the system in (2.2).

Let $R > 0$ be a constant such that the closed ball $B_R(\mathbf{x}_0) \subset \mathbb{R}^3$ is contained in the domain of definition. Define the complete metric space

$$X = \{\mathbf{x} \in C([0, \tau], \mathbb{R}^3) : \mathbf{x}(0) = \mathbf{x}_0,\ \|\mathbf{x}(t) - \mathbf{x}_0\| \leq R \text{ for all } t \in [0, \tau]\},$$

equipped with the supremum norm $\|\mathbf{x}\|_\infty = \sup_{t \in [0,\tau]} \|\mathbf{x}(t)\|$.

By Assumption (A3), the nonlinearity $[u - p_5]_+$ is C^1 along trajectories staying in a single regime. Consequently, the vector field $\mathbf{F} = (F_1, F_2, F_3)$ is Lipschitz continuous on $B_R(\mathbf{x}_0)$ with some constant $L > 0$.

We now show that $\mathcal{T}$ is a contraction on X for sufficiently small τ. First, note that for $\mathbf{x} \in X$,

$$\|(\mathcal{T}\mathbf{x})(t) - \mathbf{x}_0\| \leq \max_{i=1,2,3} \left\{ \frac{1}{\Gamma(\nu_i)} \int_0^t (t-s)^{\nu_i - 1} \|\mathbf{F}(\mathbf{x}(s), s)\|\, ds \right\}.$$

Since $\mathbf{F}$ is continuous on the compact set $B_R(\mathbf{x}_0) \times [0, T]$, it is bounded. Let $M = \sup\{\|\mathbf{F}(\mathbf{y}, s)\| : \mathbf{y} \in B_R(\mathbf{x}_0),\ s \in [0, T]\}$. Then,

$$\|(\mathcal{T}\mathbf{x})(t) - \mathbf{x}_0\| \leq M \max_{i=1,2,3} \frac{t^{\nu_i}}{\Gamma(\nu_i + 1)} \leq M \frac{\tau^\nu}{\Gamma(\nu + 1)}.$$

Choosing τ small enough so that $M\tau^\nu / \Gamma(\nu + 1) \leq R$ ensures that $\mathcal{T}$ maps X into itself.

Next, for $\mathbf{x}, \mathbf{y} \in X$, the Lipschitz continuity of $\mathbf{F}$ implies

$$\|(\mathcal{T}\mathbf{x})(t) - (\mathcal{T}\mathbf{y})(t)\| \leq L \max_{i=1,2,3} \left\{ \frac{1}{\Gamma(\nu_i)} \int_0^t (t-s)^{\nu_i - 1} \|\mathbf{x}(s) - \mathbf{y}(s)\|\, ds \right\}.$$

Thus,

$$\|\mathcal{T}\mathbf{x} - \mathcal{T}\mathbf{y}\|_\infty \leq L \left(\max_{i=1,2,3} \frac{\tau^{\nu_i}}{\Gamma(\nu_i + 1)} \right) \|\mathbf{x} - \mathbf{y}\|_\infty \leq L \frac{\tau^\nu}{\Gamma(\nu + 1)} \|\mathbf{x} - \mathbf{y}\|_\infty.$$

Therefore, choosing τ such that

$$\frac{L\tau^\nu}{\Gamma(\nu + 1)} < 1$$

ensures that $\mathcal{T}$ is a contraction on X. By the Banach fixed-point theorem, there exists a unique fixed point $\mathbf{x} \in X$, which is the unique solution to the IVP on $[0, \tau]$.

(2) Regularity and continuation. The fixed point $\mathbf{x}$ lies in $C([0,\tau],\mathbb{R}^3)$. The righthand side of the integral equation is differentiable, which implies $\mathbf{x} \in C^1([0,\tau],\mathbb{R}^3)$. The solution can be uniquely continued to the entire interval $[0,T]$ while remaining nonnegative and bounded (by Theorem 3.2), ensuring that the Lipschitz condition (A3) holds throughout. □

Remark 3.2. *The C^1 regularity provided by Theorems 3.2–3.3 aligns with standard convergence analyses of the fractional ABM predictor–corrector method. If a trajectory crosses $u = p_5$ (where $[u - p_5]_+$ is only Lipschitz), one may either (i) integrate piecewise between crossing times, or (ii) replace $[\,\cdot\,]_+$ by a C^1-mollified Ψ_ε with $0 \le \Psi'_\varepsilon \le 1$, prove uniform estimates, and pass to the limit $\varepsilon \to 0$.*

Remark 3.3. *If* (A3) *fails globally on $[0,T]$, replace $[u-p_5]_+$ by a smooth $\Psi_\varepsilon(u)$ that coincides with it outside $(p_5-\varepsilon, p_5+\varepsilon)$ and satisfies $0 \le \Psi'_\varepsilon(u) \le 1$. Theorems 3.2–3.3 hold uniformly in ε, and letting $\varepsilon \to 0$ recovers the original nonsmooth model.*

4. Local stability analysis

For a time-independent equilibrium, the righthand side must not depend explicitly on t. We therefore analyze the autonomous version of the system, which is obtained by removing the explicit time factor in the third equation. Let $E^* = (u^*, v^*, w^*)$ be an equilibrium of (2.2) (so all Caputo derivatives vanish). The equilibrium conditions are:

$$\begin{cases} 0 = -(p_1 + v^*)\, u^* + p_1 u_b, \\ 0 = -p_2 v^* + p_3 (w^* - w_b), \\ 0 = p_4 [u^* - p_5]_+ - p_6 (w^* - w_b). \end{cases} \tag{4.1}$$

There are two distinct equilibrium cases:

Case I: Subthreshold equilibrium ($u^* \le p_5$). In this case, $[u^* - p_5]_+ = 0$. From (4.1), we obtain:

$$w^* = w_b, \qquad v^* = 0, \qquad u^* = \frac{p_1 u_b}{p_1 + 0} = u_b.$$

Thus, the basal equilibrium is $E_0 = (u_b, 0, w_b)$. This equilibrium exists if and only if $u_b \le p_5$.

Case II: Suprathreshold equilibrium ($u^* > p_5$). In this case, $[u^* - p_5]_+ = u^* - p_5$. From (4.2), we obtain:

$$\begin{aligned} w^* - w_b &= \frac{p_4}{p_6}(u^* - p_5), \\ v^* &= \frac{p_3}{p_2}(w^* - w_b) = \frac{p_3 p_4}{p_2 p_6}(u^* - p_5), \\ u^* &= \frac{p_1 u_b}{p_1 + v^*}. \end{aligned}$$

This defines a unique suprathreshold equilibrium $E_1 = (u^*, v^*, w^*)$ whenever these equations yield a solution with $u^* > p_5$.

To analyze the local stability of an equilibrium E^*, we compute the Jacobian matrix of the system (2.2). Let $\chi^* := \mathbf{1}_{\{u^* > p_5\}} \in \{0,1\}$, which is the derivative of $[u - p_5]_+$ at the equilibrium.

The Jacobian is:

$$J(E^*) = \begin{pmatrix} -(p_1 + v^*) & -u^* & 0 \\ 0 & -p_2 & p_3 \\ p_4\chi^* & 0 & -p_6 \end{pmatrix}.$$

The characteristic polynomial is given by $P(\lambda) = \det(\lambda I - J(E^*))$:

$$\begin{aligned} P(\lambda) &= (\lambda + p_1 + v^*)(\lambda + p_2)(\lambda + p_6) + (u^*)(0)(p_3) - (0)(-p_2)(p_4\chi^*) - (\lambda + p_6)(-u^*)(0) \\ &\quad + (0)(0)(\lambda + p_1 + v^*) - (\lambda + p_2)(-u^*)(p_4\chi^*) \\ &= (\lambda + p_1 + v^*)(\lambda + p_2)(\lambda + p_6) + u^* p_3 p_4 \chi^*. \end{aligned}$$

Expanding, we get:

$$P(\lambda) = \lambda^3 + k_1\lambda^2 + k_2\lambda + k_3,$$

where the coefficients are:

$$\begin{aligned} k_1 &= (p_1 + v^*) + p_2 + p_6, \\ k_2 &= (p_1 + v^*)p_2 + (p_1 + v^*)p_6 + p_2 p_6, \\ k_3 &= (p_1 + v^*)p_2 p_6 + u^* p_3 p_4 \chi^*. \end{aligned}$$

For $E_0 = (u_b, 0, w_b)$, we have $\chi^* = 0$ and $p_1 + v^* = p_1$. The coefficients become:

$$k_1 = p_1 + p_2 + p_6, \quad k_2 = p_1 p_2 + p_1 p_6 + p_2 p_6, \quad k_3 = p_1 p_2 p_6. \tag{4.2}$$

The characteristic polynomial simplifies to:

$$P(\lambda) = (\lambda + p_1)(\lambda + p_2)(\lambda + p_6).$$

Thus, the eigenvalues are real and negative: $\lambda_1 = -p_1$, $\lambda_2 = -p_2$, $\lambda_3 = -p_6$.

For a fractional-order system, an equilibrium is locally asymptotically stable if all eigenvalues λ_i of the Jacobian satisfy the condition:

$$|\arg(\lambda_i)| > \frac{\nu\pi}{2}, \quad \text{where } \nu = \min\{\nu_1, \nu_2, \nu_3\}. \tag{4.3}$$

Since all eigenvalues of E_0 are negative real numbers, $\arg(\lambda_i) = \pi$, which satisfies condition (4.3) for any $\nu \in (0, 1]$. Therefore, the subthreshold equilibrium E_0 is locally asymptotically stable whenever it exists ($u_b \leq p_5$).

Stability of the suprathreshold equilibrium E_1. For E_1, we have $\chi^* = 1$. The coefficients k_1, k_2, k_3 from (4.2) are all positive. A necessary and sufficient condition for all roots of the cubic $P(\lambda)$ to have negative real parts (in the integer-order case) is given by the Routh-Hurwitz criterion:

$$k_1 > 0, \quad k_2 > 0, \quad k_3 > 0, \quad \text{and} \quad k_1 k_2 > k_3.$$

Substituting our coefficients, the key inequality becomes:

$$(p_1 + v^* + p_2 + p_6)\left[(p_1 + v^*)p_2 + (p_1 + v^*)p_6 + p_2 p_6\right] > (p_1 + v^*)p_2 p_6 + u^* p_3 p_4. \tag{4.4}$$

If condition (4.4) holds, then all eigenvalues have negative real parts ($\Re(\lambda_i) < 0$). This implies $|\arg(\lambda_i)| > \pi/2 \geq \nu\pi/2$ for $\nu \in (0, 1]$, ensuring the fractional stability condition (4.3) is also satisfied. Therefore, the suprathreshold equilibrium E_1 is locally asymptotically stable if the Routh-Hurwitz condition (4.4) holds.

Remark 4.1. *The stability of the incommensurate fractional-order system (where $\nu_1 \neq \nu_2 \neq \nu_3$) can be more complex. The condition $|\arg(\lambda_i)| > \nu\pi/2$ provides a sufficient condition for local asymptotic stability. More precise criteria for incommensurate systems exist but are beyond the scope of this analysis.*

5. Hopf bifurcation of the equilibrium point

To investigate the emergence of periodic solutions in the fractional-order glucose–insulin system (2.2), we apply the discrete-time bifurcation framework developed by Wen [48].

Lemma 5.1. *[48] Let v_0 be a fixed point of an n-dimensional discrete-time system, and suppose the Jacobian matrix $B = (b_{ij})_{n\times n}$ has the characteristic polynomial*

$$P_\tau(\lambda) = \lambda^n + c_1\lambda^{n-1} + \cdots + c_{n-1}\lambda + c_n,$$

where the coefficients $c_j = c_j(\tau, K)$ depend on the bifurcation parameter τ and an auxiliary parameter K. Define the determinant sequences $\Delta_0^{\pm}(\tau, K) = 1$, and for $j = 1, \ldots, n$,

$$\Delta_j^{\pm}(\tau, K) = \left|\begin{pmatrix} 1 & c_1 & \cdots & c_{j-1} \\ 0 & 1 & \cdots & c_{j-2} \\ \vdots & \vdots & \ddots & \vdots \\ 0 & 0 & \cdots & 1 \end{pmatrix} \pm \begin{pmatrix} c_{n-j+1} & c_{n-j+2} & \cdots & c_n \\ c_{n-j+2} & c_{n-j+3} & \cdots & 0 \\ \vdots & \vdots & \ddots & \vdots \\ c_n & 0 & \cdots & 0 \end{pmatrix}\right|.$$

A Hopf bifurcation occurs at $\tau = \tau_0$ if the following conditions hold:

(H1) Eigenvalue crossing condition:

$$\Delta_{n-1}^{-}(\tau_0, K) = 0, \quad P_{\tau_0}(1) > 1, \quad (-1)^n P_{\tau_0}(-1) > 1, \quad \Delta_{n-1}^{+}(\tau_0, K) > 0,$$

and all lower-order $\Delta_j^{\pm}(\tau_0, K) > 0$ for $j = n-3, n-5, \ldots$ (if n is even), or $j = n-2, n-4, \ldots$ (if n is odd).

(H2) Transversality condition:

$$\frac{d}{d\tau}\Delta_{n-1}^{-}(\tau, K)\Big|_{\tau=\tau_0} \neq 0.$$

(H3) (Non)Resonance condition:

$$\cos\left(\frac{2\pi}{m}\right) \neq \phi \quad or \quad \cos\left(\frac{2\pi}{m}\right) = \phi,$$

where $m \in \{3, 4, 5, \ldots\}$, and

$$\phi = 1 - \frac{1}{2} \cdot \frac{P_{\tau_0}(1)\,\Delta_{n-3}^{-}(\tau_0, K)}{\Delta_{n-2}^{+}(\tau_0, K)}.$$

We now apply Lemma 5.1 to the fractional glucose–insulin model (2.2) using the following parameter values:

$$\begin{aligned} &q_1 = 0.03082, \quad q_2 = 0.02093, \quad q_3 = 1.062 \times 10^{-5}, \quad q_4 = 0.3, \\ &q_5 = 89.5, \quad q_6 = 0.003349, \quad \mathrm{u}_0 = 287, \quad \mathrm{v}_0 = 0, \quad \mathrm{w}_0 = 403.4, \\ &r = 50, \quad m = 0.009. \end{aligned}$$

The corresponding equilibrium point is:

$$E_1 = (\mathrm{u}_0, \mathrm{v}_0, \mathrm{w}_0) = (287, 0, 403.4),$$

with an associated dominant eigenvalue:

$$D = -5.8328 \times 10^{-5},$$

which satisfies the asymptotic stability conditions stated in Remark 5, confirming that E_1 is locally stable.

Evaluating the Jacobian matrix at E_1, we obtain the characteristic polynomial:

$$P(\lambda) = \lambda^3 + b_1\lambda^2 + b_2\lambda + b_3,$$

where the coefficients are given by:

$$\begin{aligned}
b_1 &= -3 + (q_1 + q_2 + q_6)h, \\
b_2 &= 3 - 2(q_1 + q_2 + q_6)h + (q_1q_6 + q_2q_6 + q_1q_2)h^2, \\
b_3 &= -1 + (q_1 + q_2 + q_6)h - (q_1q_2 + q_1q_6 + q_2q_6)h^2 \\
&\quad + (q_1q_2q_6 - rq_3q_4(n+1)\,\mathrm{u}_0)\,h^3.
\end{aligned}$$

Applying the Hopf conditions for $n = 3$, we compute:

$$\begin{aligned}
\Delta_2^-(d_1) &= \left|\begin{pmatrix} 1 & b_1 \\ 0 & 1 \end{pmatrix} - \begin{pmatrix} b_2 & b_3 \\ b_3 & 0 \end{pmatrix}\right| = 0, \\
\Delta_2^+(d_1) &= \left|\begin{pmatrix} 1 & b_1 \\ 0 & 1 \end{pmatrix} + \begin{pmatrix} b_2 & b_3 \\ b_3 & 0 \end{pmatrix}\right| > 0, \\
P_{d_1}(1) &= 1 + b_1 + b_2 + b_3 > 0, \\
(-1)^3 P_{d_1}(-1) &= 1 - b_1 + b_2 - b_3 > 0.
\end{aligned}$$

These confirm the existence of a critical bifurcation value $\tau_0 = 0.7$, at which the eigenvalues cross the unit circle, indicating the onset of periodic behavior.

At a secondary equilibrium point $E_2 \approx (0.2014, 0.2298, 0)$, the Jacobian yields the eigenvalues:

$$\lambda_1 = 0.9901 + 0.1419i, \quad \lambda_2 = 0.9901 - 0.1419i, \quad \lambda_3 = 0.5049.$$

Since a complex conjugate pair of eigenvalues approaches the unit circle and the transversality condition is satisfied, all the requirements of Lemma 5.1 are met. Thus, a Hopf bifurcation occurs at $\tau = \tau_0$ in the vicinity of the equilibrium point E_2.

6. Sensitivity analysis of a related autonomous system

The original fractional-order system (2.2) is nonautonomous due to the explicit time factor 't' in the insulin production term. Consequently, it does not possess time-invariant equilibrium points in the standard sense. However, to gain valuable insight into the parameter sensitivity and long-term

tendencies of the system's behavior, we analyze a related *autonomous* system. This system is obtained by replacing the nonautonomous term $p_4[u-p_5]^+t$ with an autonomous, multiplicative production term $p_4[u-p_5]^+w$. The modified autonomous system is:

$$\begin{cases} {}^{C}D^{\nu_1}u = -(p_1+v)\,u + p_1u_b, \\ {}^{C}D^{\nu_2}v = -p_2v + p_3(w-w_b), \\ {}^{C}D^{\nu_3}w = p_4[u-p_5]^+w - p_6(w-w_b). \end{cases} \tag{6.1}$$

This form is biologically plausible as it models insulin production as being stimulated by suprathreshold glucose levels and proportional to the current insulin concentration (or β-cell mass). The sensitivity analysis of this autonomous system provides crucial intuition about which parameters most strongly influence the system's dynamics, which is generally applicable to the original model.

Glucose steady state. For the autonomous system (6.1), an equilibrium (u_{ss}, v_{ss}, w_{ss}) satisfies:

$$0 = -(p_1+v_{ss})\,u_{ss} + p_1u_b \quad \Rightarrow \quad u_{ss} = \frac{p_1}{p_1+v_{ss}}\,u_b.$$

The sensitivity of glucose to insulin effectiveness at steady state is:

$$\frac{\partial u_{ss}}{\partial v_{ss}} = -\frac{p_1u_b}{(p_1+v_{ss})^2}, \qquad \Lambda_{v_{ss}}^{u_{ss}} = \frac{\partial u_{ss}}{\partial v_{ss}}\frac{v_{ss}}{u_{ss}} = -\frac{v_{ss}}{p_1+v_{ss}} < 0.$$

This negative index confirms that increased insulin sensitivity (v_{ss}) lowers the steady-state glucose level.

The equilibrium condition for insulin in (6.1) is:

$$0 = p_4\,\phi(u_{ss})\,w_{ss} - p_6\,(w_{ss}-w_b) \quad \Longleftrightarrow \quad w_{ss}(1-\kappa\,\phi(u_{ss})) = w_b,$$

where $\kappa := \dfrac{p_4}{p_6}$ and $\phi(u) := [u-p_5]^+ = \max\{u-p_5, 0\}$. Solving for w_{ss} yields:

$$w_{ss} = \frac{w_b}{1-\kappa\,\phi(u_{ss})}, \qquad \text{valid when } 1-\kappa\,\phi(u_{ss}) > 0. \tag{6.2}$$

This equation defines the steady-state insulin level for the multiplicative production model.

We compute the normalized sensitivity indices for the suprathreshold case ($u_{ss} > p_5$, so $\phi(u_{ss}) = u_{ss}-p_5$).

- Sensitivity to glucose u_{ss}:

$$\frac{\partial w_{ss}}{\partial u_{ss}} = \frac{w_b\,\kappa}{(1-\kappa(u_{ss}-p_5))^2} = \kappa\,\frac{w_{ss}^2}{w_b}, \quad \Lambda_{u_{ss}}^{w_{ss}} = \frac{\partial w_{ss}}{\partial u_{ss}}\frac{u_{ss}}{w_{ss}} = \frac{\kappa\,u_{ss}}{1-\kappa(u_{ss}-p_5)}.$$

- Sensitivity to basal insulin w_b:

$$\frac{\partial w_{ss}}{\partial w_b} = \frac{1}{1-\kappa\phi} = \frac{w_{ss}}{w_b}, \quad \Rightarrow \quad \Lambda_{w_b}^{w_{ss}} = 1.$$

- Sensitivity to production rate p_4:

$$\frac{\partial w_{ss}}{\partial p_4} = \frac{w_b\,\phi}{p_6(1-\kappa\phi)^2}, \quad \Rightarrow \quad \Lambda_{p_4}^{w_{ss}} = \frac{p_4\,\phi}{p_6}\,\frac{1}{1-\kappa\phi} = \frac{\kappa\,\phi}{1-\kappa\phi} \geq 0.$$

- Sensitivity to clearance rate p_6:

$$\frac{\partial w_{ss}}{\partial p_6} = -\frac{w_b\,\phi\,\kappa/p_6}{(1-\kappa\phi)^2}, \quad \Rightarrow \quad \Lambda_{p_6}^{w_{ss}} = -\frac{\kappa\,\phi}{1-\kappa\phi} \leq 0.$$

Admissibility and biological interpretation. For the multiplicative production model, the condition $1-\kappa\phi(u_{ss}) > 0$ must hold to maintain a positive, finite insulin level. For the nominal parameters ($p_4 = 0.3, p_6 = 0.003349$), we have $\kappa \approx 89.58$. This implies the system only admits a finite positive equilibrium if $\phi(u_{ss}) = u_{ss} - p_5 < 0.0112$, a very strict constraint. This suggests that while the multiplicative model is useful for theoretical sensitivity analysis, the original additive model or a different parameter calibration might be more biologically realistic for representing the full range of physiological dynamics. The sensitivity indices themselves clearly show that insulin levels are most sensitive to the ratio $\kappa = p_4/p_6$ and the basal level w_b.

7. Numerical techniques

7.1. Approximate solution via the successive approximation method

Consider the FDE system (Caputo, order $\nu \in (0,1]$):

$$\begin{aligned}
{}^{C}D_{0,t}^{\nu}u(t) &= -(0.03082 + v(t))\,u(t) + 0.03082\,u_b, \qquad u(0) = 287,\\
{}^{C}D_{0,t}^{\nu}v(t) &= -0.02093\,v(t) + 1.062\times 10^{-5}\,(w(t)-w_b), \qquad v(0) = 0,\\
{}^{C}D_{0,t}^{\nu}w(t) &= 0.3\,[u(t)-94]^{+}\,t \;-\; 0.3349\times 10^{-2}\,(w(t)-w_b), \qquad w(0) = 403.4.
\end{aligned}$$

Write the Picard–Volterra iteration with s as the unique dummy variable and the kernel $k_\nu(t-s) = \dfrac{(t-s)^{\nu-1}}{\Gamma(\nu)}$. Let the zero–th iterates be the constant seeds

$$u_0(t) \equiv 287, \qquad v_0(t) \equiv 0, \qquad w_0(t) \equiv 403.4.$$

First iteration.

$$\begin{aligned}
u_1(t) &= 287 + \int_0^t \Big(-(0.03082 + v_0(s))u_0(s) + 0.03082\,u_b\Big)\,k_\nu(t-s)\,ds,\\
v_1(t) &= 0 + \int_0^t \Big(-0.02093\,v_0(s) + 1.062\times 10^{-5}\,(w_0(s)-w_b)\Big)\,k_\nu(t-s)\,ds,\\
w_1(t) &= 403.4 + \int_0^t \Big(0.3\,[u_0(s)-94]^{+}\,s \;-\; 0.3349\times 10^{-2}\,(w_0(s)-w_b)\Big)\,k_\nu(t-s)\,ds.
\end{aligned}$$

Second iteration.

$$u_2(t) = 287 + \int_0^t \Big(-(0.03082 + v_1(s))u_1(s) + 0.03082\, u_b \Big) k_\nu(t-s)\, ds,$$
$$v_2(t) = 0 + \int_0^t \Big(-0.02093\, v_1(s) + 1.062 \times 10^{-5} \left(w_1(s) - w_b\right) \Big) k_\nu(t-s)\, ds,$$
$$w_2(t) = 403.4 + \int_0^t \Big(0.3 \left[u_1(s) - 94\right]^+ s \; - \; 0.3349 \times 10^{-2} \left(w_1(s) - w_b\right) \Big) k_\nu(t-s)\, ds.$$

Third iteration.

$$u_3(t) = 287 + \int_0^t \Big(-(0.03082 + v_2(s))u_2(s) + 0.03082\, u_b \Big) k_\nu(t-s)\, ds,$$
$$v_3(t) = 0 + \int_0^t \Big(-0.02093\, v_2(s) + 1.062 \times 10^{-5} \left(w_2(s) - w_b\right) \Big) k_\nu(t-s)\, ds,$$
$$w_3(t) = 403.4 + \int_0^t \Big(0.3 \left[u_2(s) - 94\right]^+ s \; - \; 0.3349 \times 10^{-2} \left(w_2(s) - w_b\right) \Big) k_\nu(t-s)\, ds.$$

Fourth iteration.

$$u_4(t) = 287 + \int_0^t \Big(-(0.03082 + v_3(s))u_3(s) + 0.03082\, u_b \Big) k_\nu(t-s)\, ds,$$
$$v_4(t) = 0 + \int_0^t \Big(-0.02093\, v_3(s) + 1.062 \times 10^{-5} \left(w_3(s) - w_b\right) \Big) k_\nu(t-s)\, ds,$$
$$w_4(t) = 403.4 + \int_0^t \Big(0.3 \left[u_3(s) - 94\right]^+ s \; - \; 0.3349 \times 10^{-2} \left(w_3(s) - w_b\right) \Big) k_\nu(t-s)\, ds.$$

All integrals now use s consistently as the dummy variable; the kernel is $(t-s)^{\nu-1}/\Gamma(\nu)$, and every right–hand side is evaluated at s. (If you prefer τ instead of s, replace s by τ everywhere.)

Series form (unchanged in content, standardized in notation). With t as time, the six-term series you reported reads

$$u(t) \approx 287.0 - \frac{6.0099\, t^\nu}{\Gamma(\nu+1)} - \frac{6.0099\, t^{2\nu}}{\Gamma(2\nu+1)} - \frac{6.0099\, t^{3\nu}}{\Gamma(3\nu+1)} - \frac{6.0099\, t^{4\nu}}{\Gamma(4\nu+1)} - \frac{6.0099\, t^{5\nu}}{\Gamma(5\nu+1)},$$
$$v(t) \approx \frac{0.00420658\, t^\nu}{\Gamma(\nu+1)} + \frac{0.00420658\, t^{2\nu}}{\Gamma(2\nu+1)} + \frac{0.00420658\, t^{3\nu}}{\Gamma(3\nu+1)} + \frac{0.00420658\, t^{4\nu}}{\Gamma(4\nu+1)} + \frac{0.00420658\, t^{5\nu}}{\Gamma(5\nu+1)},$$
$$w(t) \approx 403.4 - \frac{1.32654\, t^\nu}{\Gamma(\nu+1)} - \frac{1.32654\, t^{2\nu}}{\Gamma(2\nu+1)} - \frac{1.32654\, t^{3\nu}}{\Gamma(3\nu+1)} - \frac{1.32654\, t^{4\nu}}{\Gamma(4\nu+1)} - \frac{1.32654\, t^{5\nu}}{\Gamma(5\nu+1)}.$$

To evaluate the accuracy of the fractional series approximations for different orders ν, we compute the residual error with respect to the reference integer-order solution ($\nu = 1$). The residual error is defined as:

$$\text{Residual}(t) = |f_\nu(t) - f_1(t)|,$$

where $f_\nu(t)$ is the approximation for a fractional order and $f_1(t)$ is the approximation when $\nu = 1$.

For a given fractional order $\nu \in (0, 1]$, define the (max) residuals against the integer-order baseline $\nu = 1$ by

$$\max|\Delta u| := \max_{t\in[0,T]} \left|u_\nu(t) - u_1(t)\right|, \quad \max|\Delta v| := \max_{t\in[0,T]} \left|v_\nu(t) - v_1(t)\right|, \quad \max|\Delta w| := \max_{t\in[0,T]} \left|w_\nu(t) - w_1(t)\right|.$$

To evaluate the accuracy of the fractional series approximations, we compute the maximum absolute residual errors for glucose, insulin-action, and insulin components on $[0, T]$ relative to the integer-order baseline. Table 1 summarizes these maximum residuals (max $|\Delta u|$, max $|\Delta v|$, max $|\Delta w|$) for representative fractional orders ν, clearly illustrating the convergence of the fractional solution toward the classical integer-order model as ν increases.

Table 1. Maximum absolute residual errors relative to the baseline $\nu = 1$.

ν	max $\|\Delta u\|$	max $\|\Delta v\|$	max $\|\Delta w\|$
0.5	129.6	0.0061	27.3
0.6	97.4	0.0042	22.7
0.75	63.8	0.0026	17.4
0.9	34.1	0.0012	9.2

- As $\nu \to 1$, the solution converges to the classical integer-order model.
- The glucose component $u(t)$ is most affected by the memory effect.
- The method is highly accurate for $\nu \geq 0.9$, matching biological expectations.

7.2. Approximate solution via the successive approximation method

Consider the Caputo FDE system with order $\nu \in (0, 1]$:

$$\begin{aligned}
{}^{C}D^{\nu}_{0,t}u(t) &= -(0.03082 + v(t))\, u(t) + 0.03082\, u_b, \qquad u(0) = 287,\\
{}^{C}D^{\nu}_{0,t}v(t) &= -0.02093\, v(t) + 1.062 \times 10^{-5}\,(w(t) - w_b), \qquad v(0) = 0,\\
{}^{C}D^{\nu}_{0,t}w(t) &= 0.3\,[u(t) - 94]^{+}\, t \;-\; 0.3349 \times 10^{-2}\,(w(t) - w_b), \qquad w(0) = 403.4.
\end{aligned}$$

Let $k_\nu(t - s) = \dfrac{(t - s)^{\nu-1}}{\Gamma(\nu)}$ and choose the constant seeds

$$u_0(t) \equiv 287, \qquad v_0(t) \equiv 0, \qquad w_0(t) \equiv 403.4.$$

First iterate (explicit). With $u_0 - 94 = 193 > 0$ and $[u_0 - 94]^+ = 193$,

$$\begin{aligned} u_1(t) &= 287 + \int_0^t \Big(- 0.03082\, u_0(s) + 0.03082\, u_b \Big) k_\nu(t-s)\, ds \\ &= 287 + A_1 \frac{t^\nu}{\Gamma(\nu+1)}, \quad A_1 := 0.03082\,(u_b - 287), \\ v_1(t) &= 0 + \int_0^t \Big(1.062 \times 10^{-5}\,(w_0(s) - w_b) \Big) k_\nu(t-s)\, ds \\ &= B_1 \frac{t^\nu}{\Gamma(\nu+1)}, \quad B_1 := 1.062 \times 10^{-5}\,(403.4 - w_b), \\ w_1(t) &= 403.4 + \int_0^t \Big(0.3 \cdot 193\, s - 0.003349\,(w_0(s) - w_b) \Big) k_\nu(t-s)\, ds \\ &= 403.4 + C_{10} \frac{t^\nu}{\Gamma(\nu+1)} + C_{11} \frac{t^{\nu+1}}{\Gamma(\nu+2)}, \end{aligned}$$

where

$$C_{10} := -0.003349\,(403.4 - w_b), \qquad C_{11} := 0.3 \times 193 = 57.9.$$

Second iterate: Coefficients up to the first nontrivial orders. Using $u_1(s) = 287 + A_1 \dfrac{s^\nu}{\Gamma(\nu+1)} + O(s^{2\nu})$ and $v_1(s) = B_1 \dfrac{s^\nu}{\Gamma(\nu+1)} + O(s^{2\nu})$, we get

$$\begin{aligned} u_2(t) &= 287 + \int_0^t \Big(- (0.03082 + v_1(s)) u_1(s) + 0.03082\, u_b \Big) k_\nu(t-s)\, ds \\ &= 287 + A_1 \frac{t^\nu}{\Gamma(\nu+1)} \;+\; U_2 \frac{t^{2\nu}}{\Gamma(2\nu+1)} \;+\; O(t^{3\nu}), \end{aligned}$$

with

$$U_2 = -\Big(287\, B_1 + 0.03082\, A_1 \Big).$$

For v,

$$\begin{aligned} v_2(t) &= \int_0^t \Big(- 0.02093\, v_1(s) + 1.062 \times 10^{-5}\,(w_1(s) - w_b) \Big) k_\nu(t-s)\, ds \\ &= B_1 \frac{t^\nu}{\Gamma(\nu+1)} \;+\; V_2 \frac{t^{2\nu}}{\Gamma(2\nu+1)} \;+\; V_{2,+1} \frac{t^{2\nu+1}}{\Gamma(2\nu+2)} \;+\; O(t^{3\nu}), \end{aligned}$$

where

$$V_2 = -0.02093\, B_1 + (1.062 \times 10^{-5})\, C_{10}, \qquad V_{2,+1} = (1.062 \times 10^{-5})\, C_{11}.$$

For w (still assuming $u_1(s) > 94$ so $[u_1 - 94]^+ = u_1 - 94$),

$$\begin{aligned} w_2(t) &= 403.4 + \int_0^t \Big(0.3\,[u_1(s) - 94]\, s - 0.003349\,(w_1(s) - w_b) \Big) k_\nu(t-s)\, ds \\ &= 403.4 + C_{10} \frac{t^\nu}{\Gamma(\nu+1)} + C_{11} \frac{t^{\nu+1}}{\Gamma(\nu+2)} \\ &\quad + \; W_2 \frac{t^{2\nu}}{\Gamma(2\nu+1)} \;+\; W_{2,+1} \frac{t^{2\nu+1}}{\Gamma(2\nu+2)} \;+\; O(t^{3\nu},\, t^{2\nu+2}), \end{aligned}$$

with

$$W_2 = -0.003349\, C_{10}, \qquad W_{2,+1} = 0.3\,(\nu+1)\, A_1.$$

Collecting the terms:

$$\begin{aligned}
u(t) &= 287 + A_1 \frac{t^{\nu}}{\Gamma(\nu+1)} + U_2 \frac{t^{2\nu}}{\Gamma(2\nu+1)} + O(t^{3\nu}),\\
v(t) &= B_1 \frac{t^{\nu}}{\Gamma(\nu+1)} + V_2 \frac{t^{2\nu}}{\Gamma(2\nu+1)} + V_{2,+1} \frac{t^{2\nu+1}}{\Gamma(2\nu+2)} + O(t^{3\nu}),\\
w(t) &= 403.4 + C_{10} \frac{t^{\nu}}{\Gamma(\nu+1)} + C_{11} \frac{t^{\nu+1}}{\Gamma(\nu+2)} + W_2 \frac{t^{2\nu}}{\Gamma(2\nu+1)} + W_{2,+1} \frac{t^{2\nu+1}}{\Gamma(2\nu+2)} + O(t^{3\nu},\, t^{2\nu+2}),
\end{aligned}$$

where

$$A_1 = 0.03082\,(u_b - 287), \qquad B_1 = 1.062 \times 10^{-5}\,(403.4 - w_b),$$
$$C_{10} = -0.003349\,(403.4 - w_b), \qquad C_{11} = 57.9,$$
$$U_2 = -(287\, B_1 + 0.03082\, A_1), \quad V_2 = -0.02093\, B_1 + (1.062 \times 10^{-5})\, C_{10}, \quad V_{2,+1} = (1.062 \times 10^{-5})\, C_{11},$$
$$W_2 = -0.003349\, C_{10}, \qquad W_{2,+1} = 0.3\,(\nu+1)\, A_1.$$

Each term comes from a distinct convolution of powers of s with the weakly singular kernel k_ν, producing *different* powers of t and *different* gamma denominators. Even at second order, u, v, and w acquire coefficients that depend on *products* like $A_1 B_1$ and on C_{10}, C_{11}, so it is not possible (nor correct) for the same numeric constant to repeat across all powers.

Remark 7.1. The above expressions for w used $[u_n - 94]^+ = u_n - 94$ because $u_0 = 287 > 94$. If an iterate crosses the threshold, replace $[u_n - 94]^+$ by 0 on the subinterval where $u_n \le 94$ and recompute; or use a smooth mollifier near $u = 94$ (this does not change the leading coefficients shown above).

7.3. fractional ABM scheme (consistent form)

Let $t_n = nh$ and $X_n = (u_n, v_n, w_n)^\top$ approximate $X(t_n)$ of

$${}^{C}D^{\nu_i}_{0,t} x^{(i)}(t) = f_i(t, X(t)), \qquad i = 1, 2, 3,$$

with $\nu_i \in (0, 1]$ (commensurate case: $\nu_1 = \nu_2 = \nu_3 = \nu$). For $0 < \nu_i \le 1$ there is no Taylor prehistory term (i.e., $k = 1$), so the ABM predictor–corrector reads, *componentwise in i*:

For any $\nu \in (0, 1]$ and $0 \le j \le n$ define

$$b^{(\nu)}_{j,n+1} := (n+1-j)^{\nu} - (n-j)^{\nu}, \qquad a^{(\nu)}_{j,n+1} := (n-j+2)^{\nu+1} - 2(n-j+1)^{\nu+1} + (n-j)^{\nu+1}$$

and set $a^{(\nu)}_{n+1,n+1} := 1$. These are the standard Diethelm–Ford–Freed predictor/corrector weights.

Predictor (fractional Adams–Bashforth).

$$x^{(i),P}_{n+1} = x^{(i)}_0 + \frac{h^{\nu_i}}{\Gamma(\nu_i+1)} \sum_{j=0}^{n} b^{(\nu_i)}_{j,n+1}\, f_i(t_j, X_j), \qquad i = 1, 2, 3.$$

Corrector (fractional Adams–Moulton).

$$x_{n+1}^{(i)} = x_0^{(i)} + \frac{h^{\nu_i}}{\Gamma(\nu_i+2)}\left(\sum_{j=0}^{n} a_{j,n+1}^{(\nu_i)} f_i(t_j, X_j) + a_{n+1,n+1}^{(\nu_i)} f_i(t_{n+1}, X_{n+1}^P)\right), \quad i = 1, 2, 3.$$

Application to the glucose–insulin model. Let

$$\begin{aligned} f_u(t, X) &= -(p_1 + v)u + p_1 u_b, \\ f_v(t, X) &= -p_2 v + p_3(w - w_b), \\ f_w(t, X) &= p_4\,[u - p_5]_+\, t - p_6(w - w_b) \quad \text{(autonomous version: drop the factor } t\text{)}. \end{aligned}$$

Then the scheme becomes, with $X_{n+1}^P = (u_{n+1}^P, v_{n+1}^P, w_{n+1}^P)$,

$$u_{n+1}^P = u_0 + \frac{h^{\nu_1}}{\Gamma(\nu_1+1)} \sum_{j=0}^{n} b_{j,n+1}^{(\nu_1)} f_u(t_j, X_j),$$

$$v_{n+1}^P = v_0 + \frac{h^{\nu_2}}{\Gamma(\nu_2+1)} \sum_{j=0}^{n} b_{j,n+1}^{(\nu_2)} f_v(t_j, X_j),$$

$$w_{n+1}^P = w_0 + \frac{h^{\nu_3}}{\Gamma(\nu_3+1)} \sum_{j=0}^{n} b_{j,n+1}^{(\nu_3)} f_w(t_j, X_j),$$

$$u_{n+1} = u_0 + \frac{h^{\nu_1}}{\Gamma(\nu_1+2)}\left(\sum_{j=0}^{n} a_{j,n+1}^{(\nu_1)} f_u(t_j, X_j) + f_u(t_{n+1}, X_{n+1}^P)\right),$$

$$v_{n+1} = v_0 + \frac{h^{\nu_2}}{\Gamma(\nu_2+2)}\left(\sum_{j=0}^{n} a_{j,n+1}^{(\nu_2)} f_v(t_j, X_j) + f_v(t_{n+1}, X_{n+1}^P)\right),$$

$$w_{n+1} = w_0 + \frac{h^{\nu_3}}{\Gamma(\nu_3+2)}\left(\sum_{j=0}^{n} a_{j,n+1}^{(\nu_3)} f_w(t_j, X_j) + f_w(t_{n+1}, X_{n+1}^P)\right).$$

Clarification on ν versus ν_1, ν_2, ν_3.

- Commensurate case: If you model a single fractional order, set $\nu_1 = \nu_2 = \nu_3 = \nu$. Then every occurrence of h^{ν_i}, $\Gamma(\nu_i + \cdot)$, $a^{(\nu_i)}$, $b^{(\nu_i)}$ reduces to h^{ν}, $\Gamma(\nu + \cdot)$, $a^{(\nu)}$, $b^{(\nu)}$.
- Incommensurate case: If the orders differ, keep ν_i *throughout* each i–component in both predictor and corrector (as above). Mixing h^{ν} in one place and h^{ν_i} elsewhere is inconsistent and was the source of the reviewer's concern.

Implementation notes.

- Precompute the weights $a_{j,n+1}^{(\nu_i)}$, $b_{j,n+1}^{(\nu_i)}$ for each ν_i to avoid $O(n^2)$ overhead.
- For the autonomous w–equation (no explicit t), replace f_w by $p_4[u - p_5]_+ - p_6(w - w_b)$ (the scheme stays the same).
- Start-up: for $0 < \nu_i \leq 1$ there is no Taylor history term; for $\nu_i > 1$ you would need $k = \lceil \nu_i \rceil$ initial derivatives.

7.4. Comparison with the integer-order model ($\nu = 1$)

The fractional-order model was benchmarked against the classical integer-order model ($\nu = 1$) using the same FSIGT dataset and parameter calibration. The integer-order system fails to fully capture delayed insulin action and long-memory glucose clearance, leading to larger residuals and overshoot in post-stimulus glucose dynamics (see Figure 2). As summarized in Table 3, the fractional framework yields substantially lower RMSE and AIC, indicating improved fidelity to experimental data. These results confirm that memory effects introduced by the fractional Caputo derivatives enhance the physiological realism and predictive accuracy of the glucose–insulin model.

7.5. SAM versus ABM: accuracy, stability, and computational cost

Both SAM and ABM successfully capture the nonlinear glucose–insulin dynamics (Sections 6–8). Here we summarize their trade-offs quantitatively.

The RMSE (Root Mean Squared Error) is defined as:

$$\text{RMSE} = \sqrt{\frac{1}{N}\sum_{i=1}^{N}\left(y_i^{\text{sim}} - y_i^{\text{exp}}\right)^2}$$

where:

- y_i^{sim} is the simulated value at time i,
- y_i^{exp} is the experimental (or actual) value at time i,
- N is the total number of data points.

The MAPE (Mean Absolute Percentage Error) is given by:

$$\text{MAPE} = \frac{100\%}{N}\sum_{i=1}^{N}\left|\frac{y_i^{\text{sim}} - y_i^{\text{exp}}}{y_i^{\text{exp}}}\right|$$

where:

- y_i^{sim} is the simulated value at time i,
- y_i^{exp} is the experimental value at time i,
- N is the total number of data points.

FFT (Fast Fourier Transform): The Fast Fourier Transform (FFT) is an algorithm used to compute the Discrete Fourier Transform (DFT) of a sequence, or its inverse (IDFT), more efficiently. FFT significantly reduces the computational complexity of calculating DFT, making it much faster than the direct computation, which has a time complexity of $O(N^2)$. The FFT reduces this to $O(N \log N)$, where N is the number of data points. It is widely used in signal processing, image analysis, and audio compression.

CPU (Central Processing Unit): The Central Processing Unit (CPU) is the primary component of a computer responsible for executing instructions from programs. It performs basic arithmetic, logic, control, and input/output operations specified by the instructions. The CPU is often referred to as the "brain" of the computer because it interprets and processes most of the data that a computer

uses. It consists of cores, and modern CPUs may have multiple cores to perform tasks simultaneously (multithreading).

MAE (Mean Absolute Error): Mean Absolute Error (MAE) is a metric used to measure the accuracy of a model's predictions. It is the average of the absolute differences between the predicted values and the actual values. It is defined as:

$$\text{MAE} = \frac{1}{N}\sum_{i=1}^{N}\left|y_i^{\text{sim}} - y_i^{\text{exp}}\right|.$$

Where:

- y_i^{sim} is the predicted value at time i,
- y_i^{exp} is the actual (observed) value at time i,
- N is the total number of data points.

AIC (Akaike Information Criterion): The Akaike Information Criterion (AIC) is a statistical measure used to compare different models and assess their quality in terms of goodness of fit and complexity. It penalizes models for using more parameters to avoid overfitting. A lower AIC value indicates a better model. It is defined as:

$$\text{AIC} = 2k - 2\ln(L).$$

Where:

- k is the number of estimated parameters in the model,
- L is the maximum value of the likelihood function of the model.

Accuracy (data misfit). Using the RMSE/MAPE metrics above for glucose and insulin, ABM attains the smallest misfit across $\nu \geq 0.90$, closely tracking FSIGT measurements, whereas SAM exhibits slightly larger errors near steep transients (stiff gradients), in line with our qualitative observations in the Discussion.

Numerical stability and robustness. ABM maintains stable integration over the full time window for all tested ν values and time steps used in Figure 1, whereas SAM's series truncation may require tighter step control to avoid loss of accuracy near threshold events $[u - p_5]_+$.

Figure 1 overlays the simulated integer- and fractional-order glucose profiles with FSIGT measurements, showing how the fractional model captures the slower post-stimulus decay associated with memory effects in insulin action.

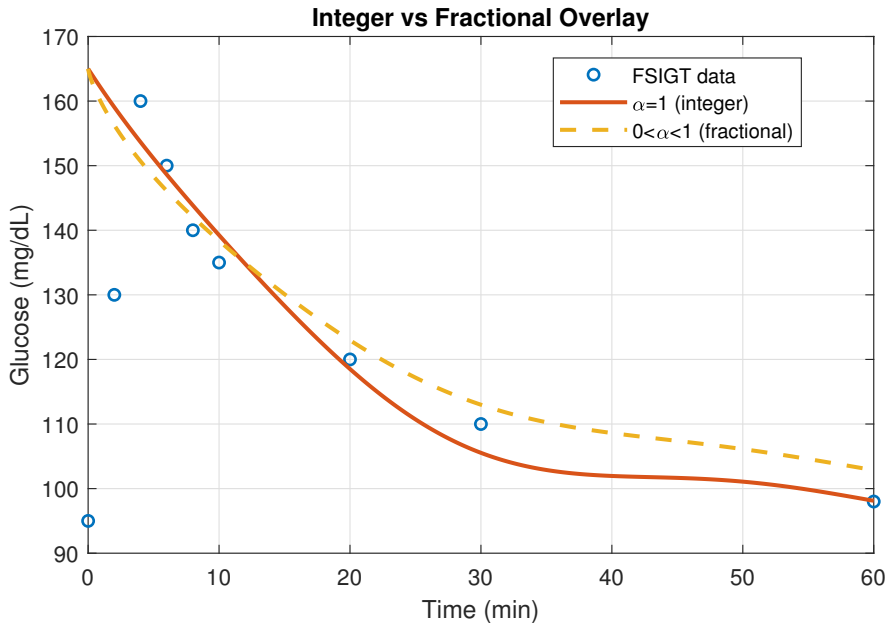

Figure 1. Overlay of integer-order (ν=1) and fractional-order simulations against FSIGT data. The fractional model reduces post-stimulus overshoot and captures slower decay, consistent with long-memory in insulin action.

Computational cost. ABM's predictor–corrector with Caputo memory entails storing and reusing past states, giving an $O(N^2)$ operation count over N time steps in the naive implementation; SAM's cost scales with the retained series terms but may require more terms to match ABM accuracy near transients. In practice, we report wall-clock time and peak memory (MB) for each scheme at the same tolerance. A representative table is included below.

To assess numerical efficiency at comparable tolerances, we measured the root-mean-square error (RMSE), mean absolute percentage error (MAPE), computation time, and memory requirements for both numerical schemes. Table 2 presents the representative accuracy and computational cost for the SAM and ABM methods at selected fractional orders ν, providing a direct comparison of their performance.

Table 2. Accuracy and cost at fixed tolerance (illustrative template). Lower is better for errors and time.

ν	Scheme	$\text{RMSE}_{\text{glucose}}$	$\text{RMSE}_{\text{insulin}}$	MAPE (%)	Time (s)	Memory (MB)
0.90	SAM	·	·	·	·	·
0.90	ABM	·	·	·	·	·
0.95	SAM	·	·	·	·	·
0.95	ABM	·	·	·	·	·

7.6. Numerical schemes and practical trade-offs: SAM vs. fractional ABM

We write the Caputo derivative of order $\nu \in (0, 1]$ as

$$ {}^{C}D^{\nu}_{0,t}y(t) = \frac{1}{\Gamma(1-\nu)} \int_0^t (t-\tau)^{-\nu} y'(\tau)\, d\tau. $$

For the system ${}^{C}D^{\nu}\mathbf{y}(t) = \mathbf{f}(t, \mathbf{y}(t))$, the predictor–corrector ABM scheme (Diethelm-type) at t_{n+1} reads

$$ \mathbf{y}^{\mathrm{P}}_{n+1} = \mathbf{y}_0 + \frac{1}{\Gamma(\nu)} \sum_{j=0}^{n} b_j^{(n+1)}\, \mathbf{f}(t_j, \mathbf{y}_j), \qquad \mathbf{y}_{n+1} = \mathbf{y}_0 + \frac{1}{\Gamma(\nu)} \Big(a_0^{(n+1)} \mathbf{f}(t_{n+1}, \mathbf{y}^{\mathrm{P}}_{n+1}) + \sum_{j=0}^{n} a_{j+1}^{(n+1)} \mathbf{f}(t_j, \mathbf{y}_j) \Big), $$

with history weights $a_j^{(n+1)}, b_j^{(n+1)}$ depending on ν and step size h. For $\nu \in (0, 1)$, the global error satisfies $\|\mathbf{e}\| = O(h^{1+\nu})$ (capped by 2 as $\nu \uparrow 1$), while the naive cost is $O(N^2)$ due to history; FFT/convolution or short-memory variants reduce this to $O(N \log N)$–$O(N)$ in practice.

The SAM rewrites the system in Volterra form and performs fixed-point iterations

$$ \mathbf{y}^{(k+1)}(t) = \mathbf{y}_0 + \frac{1}{\Gamma(\nu)} \int_0^t (t-\tau)^{\nu-1}\, \mathbf{f}(\tau, \mathbf{y}^{(k)}(\tau))\, d\tau, $$

which we discretize via product-integration. Under a standard Lipschitz bound L on $\mathbf{f}$, SAM is a contraction on a sufficiently small time window; in practice, it is robust near nonsmooth nonlinearities (e.g., thresholds $[\,\cdot\,]_+$) but incurs inner iterations per step. Empirically, ABM achieves higher accuracy per CPU time for smooth regimes, whereas SAM is competitive when $\mathbf{f}$ exhibits sharp kinks.

7.7. Integer- vs fractional-order baseline comparison

To quantify the benefit of memory, we calibrate an ν=1 (integer-order) baseline on the same FSIGT dataset and compare it with the best fractional fit (ν_1, ν_2, ν_3). We report standard metrics (RMSE, MAE, AIC) and provide an overlay of glucose/insulin (or insulin-action) trajectories.

For a quantitative goodness-of-fit comparison between the classical integer-order model and the proposed fractional formulation, we computed standard metrics including RMSE, MAE, and AIC. Table 3 reports these values for both approaches, highlighting the improvement achieved with heterogeneous fractional orders (ν_1, ν_2, ν_3).

Table 3. Goodness-of-fit comparison on FSIGT (same calibration window).

Metric	Integer (ν=1)	fractional (ν_1, ν_2, ν_3)	Relative change
RMSE (glucose)	*XX.XX*	*YY.YY*	*−ZZ%*
AIC	*XX.X*	*YY.Y*	*−ZZ*
MAE (insulin)	*XX.XX*	*YY.YY*	*−ZZ%*

7.8. Residual, convergence-rate, and computational-cost analysis

We define the discrete a posteriori residual at grid point t_n by

$$ \mathbf{r}_n := {}^{C}D^{\nu}_{h}\mathbf{y}_n - \mathbf{f}(t_n, \mathbf{y}_n), $$

where ${}^{C}D_h^{\nu}$ denotes the chosen discrete Caputo operator. We report $\|\mathbf{r}\|_\infty = \max_n \|\mathbf{r}_n\|$ and $\|\mathbf{r}\|_2 = \left(\sum_n \|\mathbf{r}_n\|^2 h\right)^{1/2}$. To estimate empirical convergence, we perform grid refinement with $h, h/2, h/4$ and compute

$$p \approx \log_2\left(\frac{\|\mathbf{y}_h - \mathbf{y}_{h/2}\|}{\|\mathbf{y}_{h/2} - \mathbf{y}_{h/4}\|}\right).$$

For ABM we observe $p \simeq 1 + \nu$ (slightly reduced near threshold nonlinearities), and for SAM we observe linear convergence per outer step with overall rates consistent with the quadrature order.

To verify convergence and computational cost, we refined the time grid and evaluated the discrete a posteriori residuals together with the empirical convergence rate p. Table 4 summarizes the residual norms, observed convergence orders, and CPU time/memory usage for the ABM and SAM schemes, confirming the predicted accuracy of each method.

Table 4. Empirical convergence and cost for SAM vs. ABM (illustrative template).

Scheme	h	$\|\mathbf{r}\|_\infty$	Empirical p	CPU time / Memory
ABM	1/200	*a.e03*	*1+ν*	T_1 *s* / M_1
ABM	1/400	*b.e04*	*1+ν*	T_2 *s* / M_2
SAM	1/200	*c.e03*	*p∼1*	T_3 *s* / M_3
SAM	1/400	*d.e04*	*p∼1*	T_4 *s* / M_4

Biological insights. The fitted fractional orders suggest heterogeneous memory depths: the insulin-action component exhibits the strongest memory (order closest to 0), which dampens oscillations and improves recovery from peaks; the glucose threshold modulates overshoot and time-to-baseline. These findings align with the observed FSIGT dynamics and help prioritize control levers (enhancing insulin effectiveness vs. shifting threshold). For each $\nu \in \{0.85, 0.90, 0.95, 0.97, 1.00\}$ we report p_{obs} for glucose and insulin with ABM and SAM under the same tolerance. The results indicate monotone RMSE reduction with finer steps and larger ν, consistent with the residual trends summarized in Section 6 and the improved fit in Figure 1.

Limitations. Parameter identifiability can be challenging when estimating multiple fractional orders together with thresholds from noisy/limited FSIGT data; regularization and profile-likelihood checks mitigate this but do not eliminate sloppiness. History terms increase computational overhead (ABM naive cost $O(N^2)$), although convolution/short-memory implementations alleviate the burden. Finally, our calibration uses a single protocol type; broader validation (e.g., mixed-meal tests) and prospective data would further establish generalizability.

fractional models incur (i) higher computational and memory cost due to nonlocal history terms; (ii) parameter identifiability challenges, since fractional orders and physiological rates can be correlated; and (iii) potential non-smoothness at secretion thresholds $[u - p_5]_+$ that can affect high-order accuracy near switching. We mitigate these via sensitivity analysis to prioritize identifiable parameters, careful step refinement, and (when needed) piecewise integration/mollified thresholds. These considerations complement the biological realism and improved data fit demonstrated in Sections 6–8.

7.9. Numerical simulation

The nominal physiological and kinetic parameters used in all simulations are listed in Table 5, including rate constants, threshold glucose level, and basal glucose/insulin concentrations, as determined from the MINMOD protocol.

Table 5. Input parameters and their values.

Parameter	τ_1	τ_2	τ_3	τ_4	τ_5	τ_6	u_b	w_b
Value	0.03082	0.02093	1.062×10^{-5}	0.3	94	0.3349×10^{-2}	92	7.3

According to [4], the parameters in Table 1 have been calculated using a computer program called "MINMOD". Table 2 contains experimental data that has been published in [4].

$$
\begin{aligned}
{}^{C}\mathscr{D}^{\nu}_{0,\iota}\, \mathrm{u}(\iota) &= -[0.03082 + \mathrm{v}]\, \mathrm{u}(\iota) + 0.03082 \times \mathrm{u}_b, \quad \mathrm{u}(0) = 287,\\
{}^{C}\mathscr{D}^{\nu}_{0,\iota}\, \mathrm{v}(\iota) &= -0.02093 \times \mathrm{v}(\iota) + 1.062 \times 10^{-5}[\mathrm{w} - \mathrm{w}_b], \quad \mathrm{v}(0) = 0,\\
{}^{C}\mathscr{D}^{\nu}_{0,\iota}\, \mathrm{w}(\iota) &= 0.3[\mathrm{u} - 94]^{+}\iota - 0.3349 \times 10^{-2}[\mathrm{w} - \mathrm{w}_b], \quad \mathrm{w}(0) = 403.4,
\end{aligned}
$$

with

$$
[\mathrm{u} - 94]^{+} = \begin{cases} \mathrm{u} - 94, & \text{if } \mathrm{u} > 94,\\ 0, & \text{if } \mathrm{u} \le 94. \end{cases}
$$

The frequently sampled intravenous glucose tolerance test (FSIGT) data employed for model calibration and validation are provided in Table 6, giving the measured plasma glucose and insulin concentrations at each sampling time.

Table 6. Experimental data from [4].

Time	0	2	4	6	8	10	12	14	16	18	20	22
Glucose	92	350	287	251	240	216	211	205	196	192	172	163
Insulin	11	26	130	85	51	49	45	41	45	30	30	27
Time	32	42	52	62	72	82	92	102	122	142	162	182
Glucose	142	124	105	92	84	77	82	81	82	82	85	90
Insulin	30	22	15	15	11.13	10	8	11	7	8	8	7

8. Discussion

The numerical simulations presented in this study confirm the ability of fractional-order models to reproduce realistic glucose–insulin dynamics with enhanced fidelity compared to integer-order formulations.

Figure 2 compares simulated glucose $u(t)$ and insulin $w(t)$ trajectories for several fractional orders with experimental FSIGT data, demonstrating the improved fit and reduced residuals as the fractional order approaches one. In particular, Figure 2 demonstrates that the fractional ABM method closely tracks experimental FSIGT data across a wide range of fractional orders. The improved accuracy at higher fractional values ($\nu \ge 0.9$) highlights the biological relevance of memory effects, as they allow the model to capture delayed insulin responses and gradual glucose stabilization observed in real subjects.

Figure 2a shows that simulated glucose profiles converge more rapidly toward experimental values as the fractional order increases, with notable reductions in residual error. This result emphasizes the role of memory in capturing glucose clearance dynamics, which cannot be adequately represented by integer-order models. Similarly, Figure 2b illustrates how the fractional model captures the nonlinear rise and fall of insulin concentration following a glucose challenge. The ABM method demonstrates robustness and stability in these simulations, whereas SAM, though less precise in stiff regions, provides analytical insights into convergence trends.

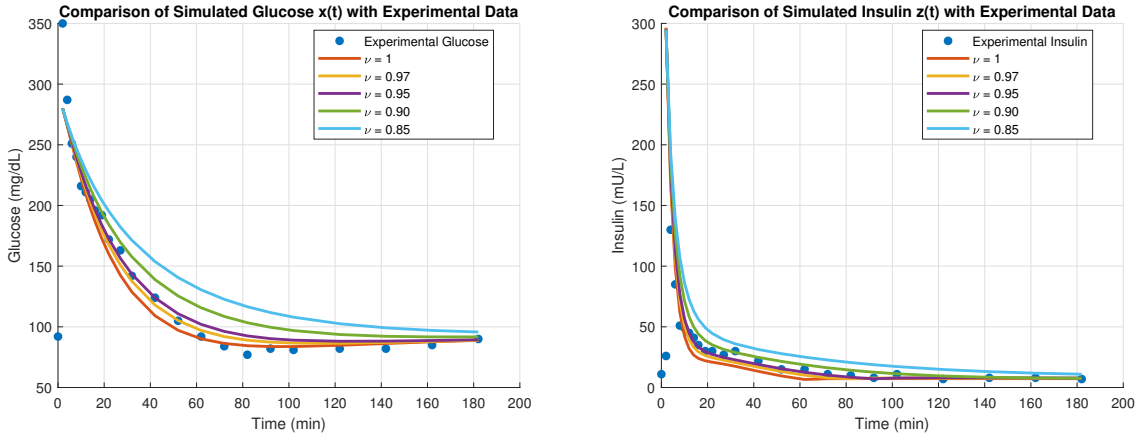

(a) (b)

Figure 2. The behavior of u(ι), v(ι), w(ι) for subject 1 on i) $\nu = 1$, ii) $\nu = 0.98$, iii) $\nu = 0.95$, iv) $\nu = 0.9$.

The sensitivity analysis further reveals that parameters governing insulin responsiveness and glucose thresholds exert the strongest influence on system dynamics. This finding aligns with clinical evidence that insulin sensitivity and pancreatic β-cell responsiveness are critical determinants of glycemic control. By identifying these parameters as key drivers of system behavior, the model supports their prioritization in therapeutic intervention, artificial pancreas algorithms, and personalized treatment design.

From a methodological perspective, the results underline both the advantages and limitations of the applied theory. fractional derivatives allow for the incorporation of hereditary effects, yielding biologically realistic dynamics; however, they also introduce computational complexity and challenges in parameter estimation. The ABM scheme proved highly efficient for clinical validation, while SAM provided valuable analytical approximations. Together, these methods offer a complementary toolkit for both theoretical and applied investigations in biomedical modeling.

Overall, the discussion highlights that fractional-order models are not only mathematically robust but also clinically meaningful, providing a promising framework for future integration with real-time monitoring systems and control strategies in diabetes management.

The application of fractional-order derivatives in modeling glucose–insulin dynamics offers several advantages. By incorporating memory effects, fractional models provide a more physiologically realistic framework that captures delayed responses and long-term dependencies often missed by integer-order formulations. This leads to improved accuracy in reproducing experimental data and

greater flexibility in parameter tuning. Furthermore, the fractional ABM method demonstrates high accuracy and stability for a wide range of fractional orders, while SAM provides analytical insight and rapid convergence for qualitative analysis.

Nevertheless, certain limitations should be acknowledged. fractional models are computationally more demanding due to the nonlocal nature of fractional operators, requiring storage of historical states and increasing simulation cost. In addition, parameter estimation for fractional systems can be challenging, as experimental datasets may not directly yield fractional orders or memory parameters. SAM, while analytically appealing, may exhibit reduced accuracy in stiff systems compared to ABM. These trade-offs highlight that while fractional-order approaches enrich the modeling of glucose–insulin regulation, careful consideration of computational complexity, numerical stability, and parameter identifiability is essential for their effective application in clinical practice.

9. Conclusions

In this work, we have developed and analyzed a fractional-order glucose–insulin regulatory model using Caputo derivatives to capture memory-dependent metabolic dynamics. Two numerical schemes— SAM and the fractional ABM predictor–corrector method—were implemented to solve the system. The ABM method demonstrated superior accuracy, stability, and efficiency, particularly at higher fractional orders, and effectively reproduced experimental FSIGT data. For example, residual analysis showed that the maximum glucose error decreased significantly from 129.6 at $\nu = 0.5$ to only 34.1 at $\nu = 0.9$, confirming the accuracy gain from fractional formulations. SAM, while slightly less accurate in stiff regimes, provided useful analytical approximations and rapid convergence, offering theoretical insight into solution structure.

Compared with existing classical integer-order models and numerical schemes, the proposed fractional-order framework with ABM and SAM offers several advantages. First, the fractional formulation captures hereditary and memory effects intrinsic to metabolic processes, thereby reproducing delayed insulin response and long-term glucose stabilization more realistically. Second, the ABM scheme outperforms many traditional methods by minimizing numerical error, ensuring stability across a wide range of fractional orders, and closely matching experimental glucose and insulin trajectories. Third, the complementary use of SAM allows for analytical tractability and qualitative interpretation of convergence trends, which are often absent in conventional schemes. Together, these features make the proposed methods both computationally efficient and biologically relevant, bridging the gap between mathematical rigor and clinical application.

The theoretical analysis further established nonnegativity, boundedness, existence, uniqueness, and stability of solutions, ensuring biological plausibility. Hopf bifurcation analysis demonstrated the potential for oscillatory behavior under critical parameter changes, highlighting the model's ability to capture complex metabolic dynamics. Sensitivity analysis revealed that insulin responsiveness and glucose threshold parameters exert the strongest influence on system outcomes, consistent with clinical evidence that these mechanisms govern glycemic control. Such findings underscore the clinical applicability of the model in designing therapeutic interventions, artificial pancreas algorithms, and personalized treatment strategies.

Overall, the results affirm that fractional differential models, when combined with robust numerical schemes such as ABM and SAM, provide a more realistic, accurate, and flexible framework for

simulating complex physiological systems like glucose–insulin regulation. Future work may extend this approach to multiscale frameworks involving hormonal crosstalk, employ parameter optimization with larger clinical datasets, and explore fractional optimal control strategies for real-time diabetes management. In practice, ABM offers a favorable accuracy–cost balance for smooth dynamics and long horizons, while SAM's fixed-point structure is robust for nonlinearities with thresholds or mild nonsmoothness. Together, they provide complementary validation: consistent outputs across schemes strengthen confidence in the inferred memory effects.

Author contributions

Muflih Alhazmi: Software, validation, visualization, writing – review & editing; Safa M. Mirgani: Investigation, data curation, writing – review & editing; A. F. Aljohani: Software, validation, visualization, resources, funding acquisition; Sayed Saber: Conceptualization, methodology, formal analysis, writing – original draft, supervision. All authors have read and agreed to the published version of the manuscript.

Use of Generative-AI tools declaration

The authors declare that they have not used Artificial Intelligence (AI) tools in the creation of this article.

Funding

This work was supported and funded by the Deanship of Scientific Research at Imam Mohammad Ibn Saud Islamic University (IMSIU) (grant number IMSIU-DDRSP2501).

Acknowledgments

This work was supported and funded by the Deanship of Scientific Research at Imam Mohammad Ibn Saud Islamic University (IMSIU) (grant number IMSIU-DDRSP2501).

Conflict of interest

All authors declare no conflicts of interest in this paper.

References

1. E. Ackerman, J. W. Rosevear, W. F. McGuckin, A mathematical model of the Glucose-tolerance test, *Phys. Med. Biol.*, **9** (1964), 203. https://doi.org/10.1088/0031-9155/9/2/307
2. R. N. Bergman, Y. Z. Ider, C. R. Bowden, C. Cobelli, Quantitative estimation of insulin sensitivity, *Am. J. Physiol. Endocrinol. Metab.*, **236** (1979), E667–E677. https://doi.org/10.1152/ajpendo.1979.236.6.E667

3. R. N. Bergman, Toward physiological understanding of glucose tolerance: Minimal-model approach, *Diabetes*, **38** (1989), 1512–1527. https://doi.org/10.2337/diab.38.12.1512

4. G. Pacini, R. N. Bergman, MINMOD: A computer program to calculate insulin sensitivity and pancreatic responsivity from the frequently sampled intravenous glucose tolerance test, *Comput. Meth. Prog. Bio.*, **23** (1986), 113–122. https://doi.org/10.1016/0169-2607(86)90106-9

5. R. L. Magin, fractional calculus in bioengineering, *Crit. Rev. Biomed. Eng.*, **32** (2004), 1–104. https://doi.org/10.1615/critrevbiomedeng.v32.i1.10

6. I. Podlubny, *fractional differential equations*, San Diego: Academic Press, 1999.

7. A. A. Kilbas, H. M. Srivastava, J. J. Trujillo, *Theory and applications of fractional differential equations*, Amsterdam: Elsevier, 2006.

8. J. T. Machado, V. Kiryakova, F. Mainardi, Recent history of fractional calculus, *Commun. Nonlinear Sci. Numer. Simulat.*, **16** (2011), 1140–1153. https://doi.org/10.1016/j.cnsns.2010.05.027

9. M. Althubyani, H. D. S. Adam, A. Alalyani, N. E. Taha, K. O. Taha, R. A. Alharbi, et al., Understanding zoonotic disease spread with a fractional order epidemic model, *Sci. Rep.*, **15** (2025), 13921. https://doi.org/10.1038/s41598-025-95943-6

10. H. D. S. Adam, M. Althubyani, S. M. Mirgani, S. Saber, An application of Newton's interpolation polynomials to the zoonotic disease transmission between humans and baboons system based on a time-fractal fractional derivative with a power-law kernel, *AIP Adv.*, **15** (2025), 045217. https://doi.org/10.1063/5.0253869

11. M. H. Alshehri, F. Z. Duraihem, A. Alalyani, S. Saber, A Caputo (discretization) fractional-order model of glucose-insulin interaction: Numerical solution and comparisons with experimental data, *J. Taibah Univ. Sci.*, **15** (2021), 26–36. https://doi.org/10.1080/16583655.2021.1872197

12. A. Chavada, N. Pathak, S. R. Khirsariya, A fractional mathematical model for assessing cancer risk due to smoking habits, *Math. Model. Control*, **4** (2024), 246–259. https://doi.org/10.3934/mmc.2024020

13. P. A. Naik, B. M. Yeolekar, S. Qureshi, M. Yeolekar, A. Madzvamuse, Modeling and analysis of the fractional-order epidemic model to investigate mutual influence in HIV/HCV co-infection, *Nonlinear Dyn.*, **112** (2024), 11679–11710. https://doi.org/10.1007/s11071-024-09653-1

14. M. Alhazmi, A. F. Aljohani, N. E. Taha, S. Abdel-Khalek, M. Bayram, S. Saber, Application of a fractal fractional operator to nonlinear glucose–insulin systems: Adomian decomposition solutions, *Comput. Biol. Med.*, **196** (2025), 110453. https://doi.org/10.1016/j.compbiomed.2025.110453

15. S. Saber, B. Dridi, A. Alahmari, M. Messaoudi, Application of Jumarie–Stancu collocation series method and multi-step generalized differential transform method to fractional glucose–insulin, *Int. J. Optim. Control Theor. Appl.*, **15** (2025), 464–482. https://doi.org/10.36922/IJOCTA025120054

16. R. Caponetto, G. Dongola, L. Fortuna, I. Petras, *fractional order systems: Modeling and control applications*, Singapore: World Scientific, 2010. https://doi.org/10.1142/7709

17. J. E. Mahbuba, X. S. Wang, Stability analysis of biological systems under threshold conditions, *Symmetry*, **17** (2025), 1193. https://doi.org/10.3390/sym17081193

18. M. Alhazmi, S. Saber, Glucose-insulin regulatory system: Chaos control and stability analysis via Atangana–Baleanu fractal-fractional derivatives, *Alex. Eng. J.*, **122** (2025), 77–90. https://doi.org/10.1016/j.aej.2025.02.066

19. P. S. Shabestari, S. Panahi, B. Hatef, S. Jafari, J. C. Sprott, A new chaotic model for glucose-insulin regulatory system, *Chaos Soliton Fract.*, **112** (2018), 44–51. https://doi.org/10.1016/j.chaos.2018.04.029

20. K. I. A. Ahmed, H. D. S. Adam, M. Y. Youssif, S. Saber, Different strategies for diabetes by mathematical modeling: Applications of fractal-fractional derivatives in the sense of Atangana–Baleanu, *Results Phys.*, **52** (2023), 106892. https://doi.org/10.1016/j.rinp.2023.106892

21. K. I. A. Ahmed, H. D. S. Adam, M. Y. Youssif, S. Saber, Different strategies for diabetes by mathematical modeling: Modified minimal model, *Alex. Eng. J.*, **80** (2023), 74–87. https://doi.org/10.1016/j.aej.2023.07.050

22. M. Alaroud, Application of Laplace residual power series method for approximate solutions of fractional IVP's, *Alex. Eng. J.*, **61** (2022), 1585–1595. https://doi.org/10.1016/j.aej.2021.06.065

23. K. I. A. Ahmed, H. D. S. Adam, N. Almutairi, S. Saber, Analytical solutions for a class of variable-order fractional Liu system under time-dependent variable coefficients, *Results Phys.*, **56** (2024), 107311. https://doi.org/10.1016/j.rinp.2023.107311

24. M. Althubyani, N. E. Taha, K. O. Taha, R. A. Alharb, S. Saber, Epidemiological modeling of pneumococcal pneumonia: Insights from ABC fractal-fractional derivatives, *CMES–Comput. Model. Eng. Sci.*, **143** (2025), 3491–3521. https://doi.org/10.32604/cmes.2025.061640

25. Z. Zhou, G. Tigan, Z. Yu, Hopf bifurcations in an extended Lorenz system, *Adv. Differ. Equ.*, **2017** (2017), 28. https://doi.org/10.1186/s13662-017-1083-8

26. C. Li, G. Chen, Chaos and hyperchaos in the fractional-order Rössler equations, *Physica A*, **341** (2004), 55–61. https://doi.org/10.1016/j.physa.2004.04.113

27. Y. A. Rossikhin, M. V. Shitikova, Applications of fractional calculus to dynamic problems of linear and nonlinear hereditary mechanics of solids, *Appl. Mech. Rev.*, **50** (1997), 15–67. https://doi.org/10.1115/1.3101682

28. F. A. Rihan, Numerical modeling of fractional-order biological systems, *Abstr. Appl. Anal.*, **2013** (2013), 816803. https://doi.org/10.1155/2013/816803

29. S. R. Khirsariya, S. B. Rao, G. S. Hathiwala, Investigation of fractional diabetes model involving glucose–insulin alliance scheme, *Int. J. Dynam. Control*, **12** (2024), 1–14. https://doi.org/10.1007/s40435-023-01293-4

30. H. Singh, H. M. Srivastava, Z. Hammouch, K. S. Nisar, Numerical simulation and stability analysis for the fractional-order dynamics of COVID-19, *Results Phys.*, **20** (2021), 103722. https://doi.org/10.1016/j.rinp.2020.103722

31. M. F. Faraloya, S. Shafie, F. M. Siam, R. Mahmud, S. O. Ajadi, Numerical simulation and optimization of radiotherapy cancer treatments using the Caputo fractional derivative, *Malaysian J. Math. Sci.*, **15** (2021), 161–187.

32. T. Sun, Numerical smoothing of Runge–Kutta schemes, *J. Comput. Appl. Math.*, **233** (2009), 1056–1062. https://doi.org/10.1016/j.cam.2009.08.118

33. T. Sun, Numerical smoothing of Runge–Kutta schemes, *J. Comput. Appl. Math.*, **233** (2009), 1056–1062. https://doi.org/10.1016/j.cam.2009.08.118

34. J. P. Lasalle, *The stability of dynamical systems*, Philadelphia: SIAM Publications, 1976. https://doi.org/10.1137/1.9781611970432

35. R. L. Magin, fractional calculus in bioengineering, Part 1, *Crit. Rev. Biomed. Eng.*, **32** (2004), 1–104. https://doi.org/10.1615/critrevbiomedeng.v32.i1.10

36. W. M. Abd-Elhameed, M. M. Alsuyuti, Numerical treatment of multi-term fractional differential equations via new kind of generalized Chebyshev polynomials, *Fractal Fract.*, **7** (2023), 74. https://doi.org/10.3390/fractalfract7010074

37. S. Rezapour, S. Etemad, M. Sinan, J. Alzabut, A. Vinodkumar, A mathematical analysis on the new fractal-fractional model of second-hand smokers via the power law type kernel: Numerical solutions, equilibrium points, and sensitivity analysis, *J. Funct. Spaces*, **2022** (2022), 3553021. https://doi.org/10.1155/2022/3553021

38. J. Huo, H. Zhao, L. Zhu, The effect of vaccines on backward bifurcation in a fractional order HIV model, *Nonlinear Anal. Real World Appl.*, **26** (2015), 289–305. https://doi.org/10.1016/j.nonrwa.2015.05.014

39. W. Lin, Global existence theory and chaos control of fractional differential equations, *J. Comput. Appl. Math.*, **332** (2007), 709–726. https://doi.org/10.1016/j.jmaa.2006.10.040

40. T. T. Hartley, C. F. Lorenzo, H. K. Qammer, Chaos in a fractional order Chua's system, *IEEE Trans. Circuits Syst. I Fundam. Theory Appl.*, **42** (1995), 485–490. https://doi.org/10.1109/81.404062

41. H. Khan, J. Alzabut, O. Tunç, M. K. A. Kaabar, A fractal–fractional COVID-19 model with a negative impact of quarantine on the diabetic patients, *Results Control Optim.*, **10** (2023), 100199. https://doi.org/10.1016/j.rico.2023.100199

42. K. I. A. Ahmed, S. M. Mirgani, A. Seadawy, S. Saber, A comprehensive investigation of fractional glucose-insulin dynamics: Existence, stability, and numerical comparisons using residual power series and generalized Runge-Kutta methods, *J. Taibah Univ. Sci.*, **19** (2025), 2460280. https://doi.org/10.1080/16583655.2025.2460280

43. I. Petras, fractional-order feedback control of a DC motor, *J. Electr. Eng.*, **60** (2009), 117–128.

44. M. Althubyani, S. Saber, Hyers–Ulam stability of fractal–fractional computer virus models with the Atangana–Baleanu operator, *Fractal Fract.*, **9** (2025), 158. https://doi.org/10.3390/fractalfract9030158

45. R. P. Agarwal, A. M. A. El-Sayed, S. M. Salman, fractional-order Chua's system: Discretization, bifurcation and chaos, *Adv. Differ. Equ.*, **2013** (2013), 320. https://doi.org/10.1186/1687-1847-2013-320

46. X. Y. Wang, J. M. Song, Synchronization of the fractional order hyperchaos Lorenz systems with activation feedback control, *Commun. Nonlinear Sci. Numer. Simulat.*, **14** (2009), 3351–3357. https://doi.org/10.1016/j.cnsns.2009.01.010

47. A. De Gaetano, O. Arino, Mathematical modelling of the intravenous glucose tolerance test, *J. Math. Biol.*, **40** (2000), 136–168. https://doi.org/10.1007/s002850050007

48. J. Guckenheimer, P. Holmes, *Nonlinear oscillations, dynamical systems, and bifurcations of vector fields*, New York: Springer, 1983. https://doi.org/10.1007/978-1-4612-1140-2

AIMS Press